# Research

# Exposure to Long- and Short-Chain Per- and Polyfluoroalkyl Substances in Mice and Ovarian-Related Outcomes: An *in Vivo* and *in Vitro* Study

Pawat Pattarawat,[1,2,3]* Tingjie Zhan,[1,2,3]* Yihan Fan,[4] Jiyang Zhang,[1,2,3] Hilly Yang,[2,3] Ying Zhang,[1,2,3] Sarahna Moyd,[5] Nataki C. Douglas,[6,7] Margrit Urbanek,[8] Brian Buckley,[2,3] Joanna Burdette,[9] Qiang Zhang,[5] Ji-Yong Julie Kim,[10] and Shuo Xiao[1,2,3]

[1]Department of Pharmacology and Toxicology, Ernest Mario School of Pharmacy, Rutgers University, Piscataway, New Jersey, USA
[2]Environmental and Occupational Health Sciences Institute (EOHSI), Rutgers University, Piscataway, New Jersey, USA
[3]Center for Environmental Exposures and Disease (CEED), Rutgers University, Piscataway, New Jersey, USA
[4]Department of Environmental Health Sciences, Fielding School of Public Health, University of California, Los Angeles, Los Angeles, California, USA
[5]Gangarosa Department of Environmental Health, Rollins School of Public Health, Emory University, Atlanta, Georgia, USA
[6]Department of Obstetrics, Gynecology and Reproductive Health, New Jersey Medical School (NJMS), Rutgers University, Newark, New Jersey, USA
[7]Center for Immunity and Inflammation, Rutgers Biomedical and Health Sciences (RBHS), Newark, New Jersey, USA
[8]Department of Medicine, Northwestern University Feinberg School of Medicine, Chicago, Illinois, USA
[9]Department of Pharmaceutical Biosciences, Center for Biomolecular Science, University of Illinois at Chicago, Chicago, Illinois, USA
[10]Department of Obstetrics & Gynecology, Feinberg School of Medicine, Northwestern University, Chicago, Illinois, USA

**BACKGROUND:** The extensive use of per- and polyfluoroalkyl substances (PFAS) has led to environmental contamination and bioaccumulation of these substances. Previous research linked PFAS exposure to female reproductive disorders, but the mechanism remains elusive. Further, most studies focused on legacy long-chain PFOA and PFOS, yet the reproductive impacts of other long-chain PFAS and short-chain alternatives are rarely explored.

**OBJECTIVES:** We investigated the effects of long- and short-chain PFAS on the mouse ovary and further evaluated the toxic mechanisms of long-chain perfluorononanoic acid (PFNA).

**METHODS:** A 3D *in vitro* mouse ovarian follicle culture system and an *in vivo* mouse model were used, together with approaches of reverse transcription–quantitative polymerase chain reaction (RT-qPCR), enzyme-linked immunosorbent assay (ELISA), RNA sequencing (RNA-seq), pharmacological treatments, *in situ* zymography, histology, *in situ* hybridization, analytical chemistry, and benchmark dose modeling (BMD). Using these approaches, a wide range of exposure levels (1–250 μM) of long-chain PFAS (PFOA, PFOS, PFNA) and short-chain PFAS (PFHpA, PFBS, GenX) were first tested in cultured follicles to examine their effects on follicle growth, hormone secretion, and ovulation. We identified 250 μM as the most effective concentration for further investigation into the toxic mechanisms of PFNA, followed by an *in vivo* mouse exposure model to verify the accumulation of PFNA in the ovary and its ovarian-disrupting effects.

**RESULTS:** *In vitro* cultured ovarian follicles exposed to long- but not short-chain PFAS showed poorer gonadotropin-dependent follicle growth, ovulation, and hormone secretion in comparison with control follicles. RT-qPCR and RNA-seq analyses revealed significant alterations in the expression of genes involved in follicle-stimulating hormone (FSH)–dependent follicle growth, luteinizing hormone (LH)-stimulated ovulation, and associated regulatory pathways in the PFNA-exposed group in comparison with the control group. The PPAR agonist experiment demonstrated that a peroxisome proliferator–activated receptor gamma (PPARγ) antagonist could reverse both the phenotypic and genotypic effects of PFNA exposure, restoring them to levels comparable to the control group. Furthermore, *in vivo* experiments confirmed that PFNA could accumulate in ovarian tissues and validated the *in vitro* findings. The BMD, *in vitro*, and *in vivo* extrapolation analyses estimated follicular rupture as the most sensitive end point and that observed effects occurred in the range of human exposure to long-chain PFAS.

**DISCUSSION:** Our study demonstrates that long-chain PFAS, particularly PFNA, act as a PPARγ agonist in granulosa cells to interfere with gonadotropin-dependent follicle growth, hormone secretion, and ovulation; and exposure to high levels of PFAS may cause adverse ovarian outcomes. https://doi.org/10.1289/EHP14876

## Introduction

The per- and polyfluoroalkyl substances (PFAS) are thousands of synthetic compounds that consist of a major carbon backbone

and at least one fluoroalkyl moiety ($C_nF_{2n+1^-}$).[1] PFAS that contain eight or more carbons are defined as long-chain PFAS, including perfluorooctanoic acid (PFOA), perfluorooctane sulfonate (PFOS), and perfluorononanoic acid (PFNA). Short-chain PFAS contain four to seven carbons, such as perfluorobutane sulfonic acid (PFBS), perfluoroheptanoic acid (PFHpA), and ammonium salt of hexafluoropropylene oxide dimer acid (HFPO-DA, or GenX), and are now increasingly manufactured and applied as alternatives.[2,3] The strong C–F bonds of PFAS render them low surface tension and thermally and oxidatively resistant.[4] Since the 1960s, PFAS have been widely used in numerous consumer and industrial products, including textiles, food packaging, cookware coating, surfactants, personal care products, and aqueous firefighting foams.[5–7] PFAS are highly resistant to environmental degradation, which has led to extensive environmental contamination and bioaccumulation[8,9] and earned them the name "forever chemicals."[4,10] Due to their health threats to humans and wildlife animals, there is a growing global environmental and public health concern.[11]

Humans are exposed to PFAS primarily through drinking water, but exposure is also possible through contaminated foods, soil, contact with PFAS-containing products, and the PFAS manufacturing process.[12–16] These exposures impact millions of residents in the United States and the larger population worldwide.[17–19] The strong C–F bonds make many PFAS rarely metabolized in human bodies

after absorption, particularly long-chain PFAS, leading to prolonged half-lives up to 8–9 y,[20,21] whereas short-chain PFAS in general have shorter half-lives.[22] Long-chain PFAS are detectable in >90% of world populations,[23–25] with blood concentrations ranging from 1 nM–222 μM.[20,25–36]

Exposure to PFAS has been related to several adverse health outcomes, such as risk of liver toxicity in rainbow trout[37] and mice,[38] cancers in renal cell carcinoma population,[39] immunotoxicity in mice,[40,41] and metabolic disorders in populations with ages ranging from 6 y to 86 y.[42] Although the adverse impacts of PFAS on reproductive health remain controversial,[28,43,44] growing epidemiological evidence suggests associations between PFAS exposure and female reproductive dysfunctions related to the ovary. These include premature ovarian failure (POF),[45,46] irregular menstrual cycles,[47] polycystic ovary syndrome (PCOS),[27,48] and infertility.[49–51] The ovary houses follicles at various stages to sustain female reproductive cycles, fertility, and overall health. The early phase of follicle activation and development is largely gonadotropin-independent, but the growth of secondary and early antral follicles is responsive to or dependent on gonadotropins, primarily the follicle-stimulating hormone (FSH) and, to a lesser extent, the luteinizing hormone (LH), and the ovulation of a fully mature preovulatory follicle is triggered by the surge of LH.[52–55] In this study, "follicle growth" denotes the development of an immature preantral follicle from the gonadotropin-dependent phase to the fully mature preovulatory antral stage, ready for ovulation. Experimental studies reported that oral exposure to long-chain PFOA and PFOS in rodents at 1–10 mg/kg (0.045–0.45 mg/kg human equivalent dose) adversely impacted ovarian cyclicity,[56–59] steroidogenesis,[60–62] and oocyte maturation.[63–66] However, the underlying mechanism remains elusive. Moreover, nearly all previous studies focused on PFOA and PFOS, the two long-chain legacy PFAS that have been gradually phased out in the United States and many other countries. Other long-chain PFAS (e.g., PFNA) and emerging short-chain PFAS (e.g., GenX and PFBS), however, may reach similar contamination levels,[2,3,67] but few have examined their impacts on female ovarian functions and reproduction.

The objective of this study was to investigate the ovarian-disrupting effects of long-chain PFAS (PFOA, PFOS, or PFNA) or short-chain PFAS (PFHpA, PFBS, or GenX) and the toxic mechanisms involved. Long-chain PFAS have been shown to exhibit longer half-lives after absorption and stronger binding affinities for target proteins, such as the peroxisome proliferator–activated receptors (PPARs), than short-chain PFAS.[22,68,69] PFAS, particularly long-chain PFAS, have been speculated to exhibit endocrine-disrupting effects by activating PPARs.[69,70] There are three PPAR subtypes: PPARα, PPARβ/δ (referred to as PPARβ below), and PPARγ. PPARγ is primarily expressed in the outer layered mural granulosa cells of maturing and preovulatory follicles and has been shown to regulate gonadotropin-dependent follicle growth and ovulation.[71–76] These facts motivated us to hypothesize that PFAS acts as a PPARγ agonist in follicular granulosa cells, as the molecular initiating event (MIE), to interfere with gonadotropin-dependent follicular functions, and that exposure to long- and short-chain PFAS may exhibit differential ovarian-disrupting effects. To test this hypothesis, we first used a 3D in vitro mouse ovarian follicle culture system to test for various human relevant concentrations of six long- and short-chain PFAS on gonadotropin-dependent follicle maturation, hormone secretion, and ovulation, and determined the ovarian toxic effects and dose–response relationship of the exposed PFAS. PFNA was then selected for in vitro exposures to determine the molecular mechanisms involved and for in vivo exposures in prepubertal mice to investigate its accumulation in the ovary and verify its ovarian toxicities observed in vitro. Our in vitro and in vivo exposure models and results provide a comprehensive understanding of the potential ovarian toxicities of PFAS.

## Materials and Methods

### Animals

Both CD-1 mouse breeding colonies for ovarian follicle isolation and in vitro PFAS exposure and 21 d old CD-1 female mice (from existing breeding colony, which were purchased from Envigo, maintained at Rutgers University) for in vivo PFAS exposure, were housed in polypropylene cages in the Animal Care Facility of Research Tower at Rutgers University. Mice were kept in temperature- ($22 \pm 1°C$), humidity- (30%–70%), and light- (12/12 light/dark cycle) controlled facilities and were provided with food (PicoLab Mouse Diet 20 EXT 5R58, Cat. No. 3003269-712; LabDiet) and water ad libitum. All animals were maintained and treated according to the National Institutes of Health (NIH) Guide for the Care and Use of Laboratory Animals and the approved Institutional Animal Care and Use Committee (IACUC) protocol at the Rutgers University.[77]

### PFAS and Other Reagents

PFOA, PFOS, PFNA, PFHpA, and PFBS were purchased from Sigma-Aldrich. GenX was purchased from Manchester Organics. Stock solutions for PFOA, PFOS, PFNA, PFHpA, and PFBS were prepared in DMSO (Sigma-Aldrich). Purities of PFAS were ≥95%, ≥95%, ≥97%, ≥97%, ≥97%, and ≥95% for PFOA, PFOS, PFNA, PFHpA, PFBS, and GenX, respectively. The stock solution for GenX was prepared in ultrapure water because it has been reported to be degradable in dimethylsulfoxide (DMSO).[78–80] Stock solutions of 250 mM were aliquoted and kept at $-80°C$. Working stocks of PFAS were diluted fresh each time in follicle culture media for in vitro exposure and in phosphate-buffered saline (PBS) for in vivo exposure, with the concentration of DMSO at 0.1%. For the in vivo exposure, we chose to use 0.1% DMSO in PBS to dissolve PFNA because 0.1% DMSO is a standard practice in most toxicological studies and is not expected to influence cell viability or functions,[81,82] which is consistent with our in vitro experiment based on the need to ensure the solubility and stability of the compounds tested.

MK886 (PPARα antagonist), GWK3787 (PPARβ antagonist), and GW9662 (PPARγ antagonist) were purchased from Selleck Chemicals. The stock solutions for all three antagonists were prepared in DMSO at a concentration of 10 mM. The stock solutions were kept at $-80°C$. Working stocks of antagonists were made fresh for every experiment. GW9662 were diluted with 0.1% DMSO in PBS for in vivo exposure.

### Selection of in Vitro PFAS Exposure Concentrations

To determine the in vitro exposure concentrations of PFAS, we searched PubMed (Supplemental Material, "Literature survey of blood concentrations for each PFAS") for previous studies that measured PFAS concentrations in human blood and follicular fluid in the past 25 y (1999–2024). We selected 14 studies that spanned different years and covered populations with different degrees of exposure to long-chain PFAS, which are summarized in Table S1. The results showed that in the general population, the blood concentrations of PFOA and PFOS ranged between 0.00001–1.379 μM, and those of PFNA ranged between 0.0004 and 0.031 μM[26–31]; the follicular fluid concentrations of PFOA and PFOS in women ranged between 0.001 and 1.44 μM, and those of PFNA ranged between 0.0002 and 0.00765 μM.[28,31,83] For people living close to the sites with high levels of PFAS contamination, their blood concentrations of PFOA and PFOS ranged between 0.001 and 54.126 μM, and

PFNA ranged between 0.0001 and 0.086 μM.[25,35,36] For people with occupational exposure (e.g., former fluorochemical occupational workers), their blood concentrations of PFOA and PFOS ranged between 0 and 222 μM,[20,32–34] and we could not identify follicular fluid or PFNA data at the time of our search. Based on these studies, we undertook our study with the assumption that PFAS in human blood and follicular fluids varies between individuals (1 nM–222 μM) depending on the degree of exposure.

In addition, we also reviewed previous studies that simultaneously measured PFAS in the blood and follicular fluid. In two previous studies by Kang et al.[31] and Heffernan et al.,[28] the serum and follicular fluid concentrations of a variety of PFAS were simultaneously measured in the same individuals, and the authors found them to be highly positively correlated (linear regression model was used for correlation analysis, $p < 0.05$). In Kang et al.,[31] the median follicular fluid:serum partition coefficients of 16 PFAS compounds were between 0.47 and 0.96, with PFOA, PFOS, and PFNA at 0.76, 0.7, and 0.71, respectively. In Heffernan et al.,[28] the mean follicular fluid:serum partition coefficients of PFOA, PFOS, and PFNA were 0.78, 0.59, and 0.77, respectively.

These results suggest that the serum concentrations of PFAS of major concern can be used as a reasonable estimate for their follicular fluid concentrations, with a slight tendency toward overestimation in most exposure conditions. Because the human serum concentrations or follicular fluid concentrations of PFAS are within the range of 1 nM–222 μM in different populations,[33] we used 250 μM as the highest tested concentration in our *in vitro* follicle culture experiment, which is primarily relevant to individuals with occupational exposure rather than the general population. In addition, due to the remarkable interindividual difference of PFAS concentration in the blood and follicular fluid (Table S1), we also tested lower concentrations at 1, 10, and 100 μM to cover lower exposures and obtain the dose–response relationship between PFAS and the ovarian end points we examined.

### In Vitro *3D eIVFG, Ovulation, and PFAS Exposure*

Mouse ovaries were collected from 16-d-old CD-1 female mice. Mice were euthanized using $CO_2$ inhalation method for ovary collection. Two ovaries were collected from each mouse. The collected ovaries were then incubated in an enzymatic solution of L15 media (Invitrogen) with 30.8 μg/mL liberase (Sigma-Aldrich) and 200 μg/mL DNase I for 25 min, with agitation on a plate shaker in a 37°C incubator (Thermo Fisher Scientific). Immature preantral follicles of the size of 150–180 μm released by the enzyme solution were isolated under microscope using mouth pipette. This procedure enabled us to obtain ~150 follicles in total from 3–5 prepubertal mice (6–10 ovaries), because the number of secondary follicles per mouse varies. Ovaries were combined from those mice for the isolation of immature preantral follicles. Isolated follicles from each mouse were pooled together then were encapsulated for *in vitro* culture as we previously described.[84,85] In brief, follicles were encapsulated in 0.5% (w/v) alginate hydrogel (Sigma-Aldrich).[180] Encapsulated follicles were individually cultured in 96-well plates with each well containing a single follicle and 100 μL growth media consisting of 50% αMEM Glutamax (Thermo Fisher Scientific) and 50% F-12 Glutamax (Thermo Fisher Scientific) supplemented with 3 mg/mL bovine serum albumin (BSA; Sigma-Aldrich), 10 mIU/mL human recombinant FSH (rFSH; Organon, gifted by Dr. Mary Zelinski from the Oregon Nonhuman Primate Research Center at the Oregon Health and Science University, Beaverton, Oregon, USA), 1 mg/mL bovine fetuin (Sigma-Aldrich), and 5 μg/mL insulin-transferrin-selenium (ITS; Sigma-Aldrich). Follicles were cultured for 6 d at 37°C in a humidified environment of 5% $CO_2$ in the air, which allowed immature follicles to grow from the multilayered secondary stage to the antral stage to reach maturation. On day 6 of encapsulated *in vitro* follicle growth (eIVFG), mature antral follicles were freed from alginate by incubating them in L15 media containing 1% fetal bovine serum (FBS) and 10 IU/mL alginate lyase (Sigma-Aldrich) at 37°C for 10 min. The follicles were then transferred to ovulation-induction media, which consisted of 50% αMEM Glutamax and 50% F-12 Glutamax, supplemented with 10% FBS, 1.5 IU/mL human chorionic gonadotropin (hCG) (Sigma-Aldrich), and 10 mIU/mL rFSH. Ovulation was assessed using an Olympus inverted microscope with 10× objective (Olympus Optical Co. Ltd.) with Tcapture imaging software (version 5.1.1; Tucsen) at 14 h after hCG treatment. A follicle was classified as "ruptured" if one side of the follicular wall was breached, and as "unruptured" if the follicular wall remained intact.

In this study, no fertilization or activation experiment was performed; thus the oocytes remained at the metaphase II (MII) stage. Oocytes with the first polar body extrusion were defined as MII oocytes, indicating the resumption of meiosis I and arrest at the MII of meiosis II. This stage refers to as "Meiotic resumption." Most of the non-MII oocytes without the polar body extrusion were at either the germinal vesicle breakdown (GVBD) or the germinal vesicle (GV) stage, which were defined by the absence or presence of GV, respectively.

Follicles treated with hCG for ovulation induction were cultured in the ovulation-induction media without FSH for an additional 48 h to promote luteinization and progesterone secretion. The conditioned ovulation-induction media was collected after 48 h and stored at −20°C for subsequent progesterone measurement using ELISA.

All encapsulated follicles were randomly assigned to various experimental groups, with each group containing 10–15 follicles sourced from 3–5 mice. Each follicle was cultured individually in the wells of a 96-well plate, with each well containing 100 μL of growth media. For FSH-dependent follicle development window exposure, PFAS was added on day 2 of culture; then follicles were observed until day 6. For hCG-induced ovulation window exposure, PFAS was added on day 6 of culture for 48 h. Each concentration of each PFAS was exposed to 10–15 follicles as biological replicates, with a total of 50–75 follicles exposed to the 5 tested concentrations of each PFAS (0–250 μM). Follicles were then subjected to a tiered toxicity testing pipeline defined as follows: Tier 1 involved ovarian toxicity testing as an initial screening phase, where follicles were exposed to various concentrations of long-chain PFAS (PFOA, PFOS, or PFNA) or short-chain PFAS (PFHpA, PFBS, or GenX) at 1, 10, 100, and 250 μM during both the follicle growth window (days 2–6) and the ovulation window (days 6–7) to identify any significantly altered ovarian end points. Tier 2 focused on a specific exposure window, with follicles treated with PFAS either during the follicle maturation window (days 2–6) or the ovulation window (days 6–7) to determine the timing and specific ovarian effects of PFAS. Tier 3 comprised mechanistic studies using both *in vitro* follicle culture model and *in vivo* mouse exposure model to determine the molecular mechanisms of PFNA-induced ovarian toxicities observed in Tiers 1 and 2.

During eIVFG, half of the follicle culture media was replaced every other day, and the conditioned follicle culture media were used for measuring the steroid hormone concentrations using ELISA. Follicles were imaged at each media change every other day using the 10 × objective of the Olympus inverted microscope for evaluating follicle survival and size. Follicle death was defined by the morphological changes of oocytes with shrinkage, irregular shape, and/or fragmentation, and/or morphological changes of follicles with darker and/or disintegrated somatic cell layers. The follicle size was determined by averaging two perpendicular

measurements from one side to another side of the theca externa per follicle using the ImageJ software (version 1.53; NIH).

### Hormone Assay

The concentrations of 17β-estradiol (E₂), testosterone (T), and progesterone (P4) in the follicle culture media was measured using ELISA kits [Cayman Chemical, Research Resource Identifier (RRID): AB_2832924, Cat. No. 501890 for E₂ ELISA kit; RRID: AB_2811273, Cat. No. 582601 for P4 ELISA kit; RRID: AB_2895148, Cat. No. 582701 for T ELISA kit] according to the manufacturer's instructions. The ELISA kits we used have also been widely used in hormone detection in many mouse-related studies.[86,87] The mouse anti-rabbit IgG precoated wells were incubated with standards, conditioned follicle culture media, rabbit antiserum, and hormone-acetylcholinesterase (AChE) conjugated for 60–120 min. After the wells were washed with washing buffer three times, Ellman's reagent was added and incubated at room temperature for 60–90 mins, and the absorbance was measured using a BioTek SpectraMax M3 microplate reader (BioTek Instruments) at 414 nm within 15 min. The reportable ranges of the $E_2$, T, and P4 assays were 0.61–10,000, 3.9–500, and 7.8–1,000 pg/mL, respectively. The lower limit of detection (LOD) of $E_2$ and T were 6 and 5 pg/mL, respectively (no reported LOD for P4). The sensitivity of $E_2$, P4, and T were 20 pg/mL, 10 pg/mL, and 6 pg/mL, respectively. Interassay variability (CV) of $E_2$, P4, and T were 8%–12.3%, 1.5%–16.4%, and 2.8%–14.2%, respectively. The intra-assay variability (CV) of $E_2$, P4, and T were 6.5%–12.1%, 4.9%–54.5%, and 4.4%–19.1%, respectively. The cross-reactivity among $E_2$, P4, and T was <0.14%. Experimental controls, blanks, and series of positive standards were measured every time to ensure the accuracy of hormone levels. There were $n = 8$ follicles for each group of treatments, each experiment was repeated three times.

### In Situ *Zymography*

*In situ* zymography is a technique used to study the activities of matrix metalloproteinases (MMPs) enzymes in fixed tissue samples. Follicles from day 6 of eIVFG were incubated in the growth media with 250 μM PFNA ($n = 8$ follicles) or DMSO (vehicle control, $n = 8$) for 2 h, then transferred to the ovulation-induction media containing 100 μg/mL fluorescent-conjugated DQ gelatin (Invitrogen) with the same concentration of PFNA and incubated at 37°C in a humidified atmosphere of 5% $CO_2$ in air for 15 h. After incubation, follicles were fixed with 3.8% paraformaldehyde (PFA) at 37°C for 1 h, then stained with fluorescent DNA stain 4′,6-diamidino-2-phenylindole (DAPI) and mounted for visualization. After proteolytic digestion by MMPs, the bright green fluorescence of the DQ gelatin can be used to measure enzymatic activity. Fluorescent images of the DQ gelatin were obtained using the EVOS cell imaging system (Thermo Fisher Scientific) at an excitation wavelength of 495 nm and a detection wavelength of 515 nm.

### Single-Follicle RNA-Seq Analysis

RNA sequencing (RNA-seq) was performed to investigate the effects of PFNA on follicular transcriptomic profiling during FSH-stimulated follicle growth or hCG-induced ovulation. Follicles were treated with vehicle ($n = 10$) or 250 μM PFNA ($n = 9$, from 3–5 mice) either day 2–6 of eIVFG or for 4 h during hCG-induced *in vitro* ovulation. Follicles at the end of either exposure window were collected, and total RNA was extracted using the Arcturus PicoPure RNA isolation kit (Applied Biosystems) according to the manufacturer's instructions. Quality and quantity of RNA were initially checked with Nanodrop (Thermo Fisher Scientific). RNA samples were sent to Novogene Corporation for cDNA synthesis,

library preparation, and sequencing. The cDNA synthesis and library preparation were performed using the NEBNext Ultra II RNA Library Prep Kit for Illumina (New England Biolabs) following the manufacturer's protocol. Sequencing was conducted using low-input RNA-seq on an Illumina NovaSeq PE150 platform. Library quantification was carried out using Qubit fluorometric analysis (Thermo Fisher Scientific). There were 9–10 follicles in each group from 3–5 mice to consider the biological variance between follicles within a group in one technical replicate. The transcriptomic results were further confirmed using other measures to ensure that there was no bias, such as follicle diameter, ovulation, oocyte meiosis, hormone secretion, and expression of follicle maturation or ovulation-related genes, which were included with three independent technical replicates.

High-quality trimmed paired sequencing reads were uploaded into the Partek Flow software (version 10.0; Partek Inc.) for RNA-seq data analyses. The potential rDNA and mtDNA contaminants were filtered using Bowtie 2 (version 2.5.0), which is a highly efficient alignment tool. The filtered reads were aligned to the whole mouse genome assembly mm10 using the HISAT 2 aligner (version 2.2.1), which is integrated within the Partek workflow, to enable efficient and splice-aware alignment of RNA-seq data. Raw read counts were obtained by quantifying aligned reads to transcript annotations from Ensembl Transcripts (release 99) using the Partek EM algorithm and then normalized based on the Transcripts Per Million (TPM) method. Pseudo genes were filtered out using the list of protein encoding genes from the Human Genome Organization (HUGO) Gene Nomenclature Committee (release 7 January 2022).[88,89] Principle component analysis (PCA) was performed using the PCAtools open-source package (version 2.14.0; https://github.com/kevinblighe/PCAtools). Differential expression analysis was performed using DESeq2(R), an R package designed for analyzing RNA-seq data to identify genes with significant differences in expression across conditions. Genes with an absolute fold change ≥ 2.0 or ≤ 0.5 and a false discovery rate (FDR) adjusted $p < 0.05$ were defined as significantly differentially expressed genes (DEGs). DEGs from PFNA-exposed follicles (PFNA treatment vs. control) were compared to our previously published DEGs from 4 h post hCG–treated follicles (4-h treatment vs. 0-h treatment).[90] Gene ontology (GO) analyses were performed using Database for Annotation, Visualization, and Integrated Discovery (DAVID; version 6.8).[91] Kyoto Encyclopedia of Genes and Genomes (KEGG) pathway enrichment analysis (release July 2022) was performed on cluster-associated genes using WEB-based GEne SeT AnaLysis Toolkit (WebGestalt).[92] PPARgene list was obtained from the PPARgene database (http://www.ppargene.org/; database searched: 5 August 2022).[93]

### Mouse Superovulation, PFNA Exposure in Vivo*, and Oocyte and Ovary Collection*

An *in vivo* mouse superovulation model was used to investigate the effects of PFNA on gonadotropin-dependent follicle growth and ovulation. Because PFAS accumulate in ovaries and have long half-lives, the exposure window of PFNA covered both FSH-stimulated follicle growth and LH/hCG-induced ovulation to recapitulate the real-world continuous exposure to PFAS in women. The administration route of PFAS via intraperitoneal injection (IP), a method for delivering the chemicals directly into the peritoneal cavity for efficient absorption, was selected based on a previous study from Wang et al.,[94] which demonstrated that the short-term administration of PFAS through IP at 5–25 mg/kg was comparable to the bioaccumulation of PFAS observed in long-term human exposure through contaminated drinking water or occupational exposure, with the calculated mouse serum concentrations of PFOS at 1,075, 3,225, and 5375 ng/mL in mice treated with 5, 15, and 25 mg/kg PFOS for

5 d, respectively. These concentrations are within the range of PFAS detected in human blood serum, which was from 1 ng/mL–92,030 ng/mL.[20,23–25,31–34,94,95] Based on these previous studies, we performed an *in vivo* acute exposure to 1, 5, and 25 mg/kg PFNA via IP using 21-d-old mice for 5 d. The IP route was also considered less stressful and safer for rodents, particularly for repetitive exposure studies.[96,97] In addition, the metabolic fates of administered compounds through IP are similar to those of oral administration, because compounds need to pass through the liver before distributing to other organs in both dosing scenarios.[97,98] Thus, the exposure route of IP and a dose range of 5–25 mg/kg were used in the *in vivo* PFAS exposure experiments.

Twenty-one-day-old CD-1 female mice were selected for the superovulation induction because *a*) the CD-1 mouse strain is one of the most common outbred strains used for studying female reproductive toxicology, and it has been demonstrated that CD-1 mice are sensitive to ovarian toxic chemicals, such as doxorubicin (DOX),[99,100] bisphenol A (BPA),[101] phthalate,[102,103] methoxychlor (MXC),[104–107] genistein,[108,109] dioxin,[110] and 2,3,7,8-tetrachlorodibenzo-*p*-dioxin (TCDD),[111] etc.[112–114]; *b*) prepubertal mice at 21-d-old are commonly used for superovulation induction and oocyte retrieval for studying oocyte biology[115,116] because their ovaries have an adequate number (>20) of early antral follicles that are sensitive to exogenous gonadotropins for the induction of follicle growth, ovulation, and resumption of oocyte meiosis I; and *c*) the absence of ovarian cyclicity allows for better control and synchronization of exogenous gonadotropin-stimulated follicle growth and ovulation.

To investigate the effects of PFNA exposure on ovulation, 21-d-old mice were randomly assigned into different treatment groups and were treated with $1 \times$ PBS ($n = 15$) or 5 ($n = 13$), 15 ($n = 8$), or 25 mg/kg ($n = 9$) PFNA through IP injection daily for 5 d. On day 3, mice were injected intraperitoneally with 5 IU of pregnant mare serum gonadotropin (PMSG; ProSpec) to stimulate the growth of early antral follicles to grow to the preovulatory stage to reach full maturation. Forty-six hours after PMSG injection, mice were injected intraperitoneally with 5 IU of hCG (Sigma-Aldrich) to induce ovulation. Mice were sacrificed at 14 h post hCG injection using $CO_2$ inhalation, and oocytes were collected from the ampulla region of both sides of oviducts. The numbers of ovulated oocytes were counted and recorded, and ovaries were collected for histology.

To investigate the effects of PFNA on the expression of genes crucial for ovulation, 21-d-old CD-1 female mice received the same regimen of PMSG and hCG treatments for ovulation induction as described above. Mice were randomly assigned into two groups and were treated with $1 \times$ PBS ($n = 5$) or 25 mg/kg PFNA ($n = 5$) through IP injection daily for 5 d. Mice were sacrificed at 4 h post hCG injection, and both sides of the ovaries were collected. The follicular fluid of each ovary was collected in ultrapure water by poking large antral follicles under the microscope. One ovary from each mouse was used for isolating large antral follicles and follicular somatic cells for RT-qPCR, and the other ovary was used for *in situ* RNA hybridization.

To determine the effects of pharmacological inhibition of PPARγ on PFNA-induced ovulation failure, 21-d-old prepubertal CD-1 female mice received the same regimen of PMSG and hCG treatments as those described above. A PPARγ antagonist (GW9662) was used at a dose of 1 mg/kg.[117–119] Mice were randomly assigned into four groups and were treated with $1 \times$ PBS ($n = 8$), 1 mg/kg PPARγ antagonist (GW9662) ($n = 5$), 25 mg/kg PFNA ($n = 8$), or cotreated with 25 mg/kg PFNA and PPARγ antagonist (GW9662) (1 h before PFNA; $n = 9$), through IP injection. Mice were sacrificed at 14 h post hCG injection to count the numbers of ovulated oocytes on both sides

of oviducts under Olympus inverted microscope with $10 \times$ objective as described above.

### RNA Extraction and RT-qPCR

For the *in vitro* exposure experiment, follicles collected on day 6 of eIVFG were used to examine the expression of genes related to follicle growth and ovarian steroidogenesis, and follicles collected at 4 h post hCG were used to examine the expression of ovulatory genes using RT-qPCR, because the majority of LH/hCG target genes are highly induced at 4 h in both *in vivo* and *in vitro* ovulation models.[90,120] For *in vivo* exposure studies, somatic cells from four isolated large antral follicles in each mouse ovary ($n = 5$) collected at 4 h post hCG) were pooled together. Total RNA of each follicle or pooled follicular somatic cells were extracted using the PicoPure RNA isolation kit. RNA purity (A260/A280 ratio), and quantification of RNA were performed using NanoDrop. Total RNA was then reverse transcribed into cDNA using the Superscript III First-Strand Synthesis System with random hexamer primers (Invitrogen, Cat. No. 18080400) and stored at $-80°C$. The RT-qPCR was performed in 384-well plates using the Power SYBR Green PCR Master Mix (Thermo Fisher Scientific) in a ViiA 7 Real-Time PCR System (Thermo Fisher Scientific). RT-qPCR thermocycle was programmed for 10 min at 95°C, followed by 40 cycles of 15 s at 95°C and 40 s at 60°C, and ended with a melting curve stage to determine the specificity of primers. The relative gene expression levels of each gene were normalized by the expression of glyceraldehyde-3-phosphate dehydrogenase (*Gapdh*). Follicle growth (*Fshr*, *Lhcgr*, *Ccnd2*, *Pcna*, *Pappa*, *Inha*, *Inhba*, and *Inhbb*), steroidogenesis (*Star*, *Cyp11a1*, *Cyp17b1*, *Cyp19a1*, *Hsd3b1*, and *Hsd17b1*), and ovulation-related genes (*Ptgs2*, *Has2*, *Tnfaip6*, *Areg*, *Ereg*, *Btc*, *Adamts1*, *Plat*, *Plau*, and *Il6*) were included. The primer sequences of all examined genes are listed in Table S2. There were $n = 8$ follicles per group of treatment. Each experiment was repeated three times.

### Histology and *in Situ* Hybridization

Ovaries were fixed in 10% formalin overnight, embedded in paraffin, and serially sectioned at 5 μm. Ovarian sections were stained with hematoxylin and eosin (H&E; Thermo Fisher Scientific) for histological examination of unruptured large antral follicles.

*In situ* hybridization was performed using ovarian sections at 4 h post hCG injection to examine the expression of ovulatory genes using the RNAscope Multiplex Fluorescent Detection Kit V2 and the HybEZ Hybridization System (Advanced Cell Diagnostics, Inc.) following the manufacturer's instructions. In brief, ovarian sections underwent pretreatment with heat, hydrogen peroxide, and protease before hybridization with target gene probes for tumor necrosis factor alpha-induced protein 6 (*Tnfaip6*, Cat. No. 507491; Advanced Cell Diagnostics), steroidogenic acute regulatory protein (*Star*, Cat. No. 543581; Advanced Cell Diagnostics), and prostaglandin-endoperoxide synthase 2 (*Ptgs2*, Cat. No. 316621; Advanced Cell Diagnostics) with the volume of 50:1:1 at 40°C for 2 h. Subsequently, a horseradish peroxidase (HRP)-based signal amplification system (reagents from the RNAscope Multiplex Fluorescent Detection Kit V2, Cat. No. 323110) was applied to the target probes at 40°C for 15 min, followed by fluorescent dye labeling (Opal 520, Cat. No. FP1487001KT; Opal 570, Cat. No. FP1488001KT; Opal 690, Cat. No. FP1497001KT; Akoya Bioscience) at 40°C for 30 min. The ovary sections were mounted with VECTASHIELD Antifade Mounting Medium with DAPI (Vector Laboratories, Inc.) and then imaged using a confocal microscope (Leica).

## Analytical Measurement of Ovarian PFNA

Ovarian accumulation of PFNA in prepubertal mice treated with PBS ($n = 3$) or 1, 5, and 25 mg/kg PFNA ($n = 3$–4) through IP injection daily for 5 d was determined at 4 h post hCG injection. The vehicle, PFNA, and gonadotropin treatment regimen were the same as described above. Sample preparation and extraction followed the protocol in a previous study by Tatum-Gibbs et al. with minor modifications.[121] In brief, one ovary from each vehicle or PFNA-treated mouse was fully homogenized in 100 μL ultrapure water, and the other ovary was placed in 100 μL ultrapure water, and all PMSG-stimulated large antral follicles ($\sim 20$ follicles) were sampled with a fine needle to release the follicular fluid into the water. The volume of antral follicles was calculated using the following formula: volume of FF inside the antral cavity $(mm^3)$ = volume of antral cavity $[4/3\pi \times (Dac/2)3]$ $(mm^3)$-volume of cumulus-oocyte complex (COC) $[4/3\pi \times (Dcoc/2)3]$ $(mm^3)$. For analytical sample preparation, the ovary homogenates or follicle fluid solutions were added with 100 μL of 0.1 M formic acid and 1 mL of acetonitrile and then vigorously mixed for 15 min and centrifuged at $12,000 \times g$ for 15 min at room temperature. Then, 500 μL of the supernatant was transferred to an high-performance liquid chromatography (HPLC) sampling vial. Matrix-matched standard curves were prepared by externally spiking PFNA into the appropriate ovary matrix collected from untreated mice. The extraction method for PFNA standards was the same as above. The range of the standard curve was 0–100 ng/mg of ovary weight. Before extraction, deuterated bile acid (BA) was added to all samples as an internal standard because of its similar retention time and molecular weight with PFNA. Then, 62.5 ng BA of β-muricholic acid-d4 (β-MCA-d4) was spiked into each sample to monitor the extraction efficiency and sample loss during sample preparation and detection.

PFNA was measured using a Dionex UltiMate 3000 ultra-high-performance liquid chromatography (UHPLC) system (Thermo Fisher Scientific) coupled with a Q Exactive HF Hybrid Quadrupole-Orbitrap mass spectrometer equipped with an electrospray ionization (ESI) source (UHPLC–high resolution mass spectrometry, or UHPLC-HRMS). Chromatographic separation was conducted on a Kinetex Core-Shell C18 column ($50 \times 3$ mm, 1.7 μm; Phenomenex) at 30°C. The injection volume of the samples was 5 μL. A mobile phase of $H_2O$ with 5 mM ammonium acetate (solvent A) and methanol with 5 mM ammonium acetate (solvent B) was used, following a 15-min linear gradient elution: 0/5, 5/85, 10/100, 13.5/100, 13.51/5, 15/5 (min/B%) at a flow rate of 350 μL/min. Nitrogen was used for all gas flows. Data was collected in negative ESI mode using parallel reaction monitoring (PRM) acquisition mode. Collision energy was set to 15 for the PFNA precursor ion of 462.9635 $m/z$. PFNA product ions of 168.99, 218.99, and 418.97 $m/z$ were monitored for analyte identification and quantification. Data acquisition and processing were carried out with Thermo Xcalibur (version 4.0.27.19; Thermo Fisher Scientific) software. A solvent blank (HPLC grade acetonitrile) was carried out after six samples to monitor for any background contamination.

## Benchmark Dose Modeling

The US Environmental Protection Agency (US EPA) Benchmark Dose Modeling (BMD) Software (BMDS) tool (online version 2023.03.1)[122] was used to perform the frequentist BMD modeling and determine the point-of-departure (PoD) for end points examined in both *in vitro* and *in vivo* exposure models, including follicle growth, ovulation, oocyte meiosis I resumption, and hormonal secretion of $E_2$, P4, and T for *in vitro* exposure to PFAS with significant toxicity, and ovulation for *in vivo* exposure to PFNA. For dichotomous data, such as failure of follicle rupture, ovulation, and oocyte meiosis I resumption, the 10% extra risk of these end points

was set as the benchmark response ($BMR_{10}$) level to derive the benchmark dose/concentration ($BMD_{10}$ or $BMC_{10}$) and the corresponding 95% lower confidence limit ($BMDL_{10}$ or $BMCL_{10}$). For continuous data, such as hormone secretion and follicle diameter, a relative deviation of 10% from the background level was set as BMR, and both the constant and nonconstant variance cases were explored. The default model selection and restriction were used: for dichotomous data, the *Dichotomous Hill*, *Gamma*, *Log-Logistic*, *Multistage*, and *Weibull* models were run restricted, and the *Logistic*, *Log-Probit*, *Probit* and *Quantal Linear* models were run unrestricted; for continuous data, the *Exponential*, *Hill*, *Polynomial*, and *Power* models were run restricted, and the Linear model was run unrestricted. Selection of the best models followed the US EPA recommended guideline to determine $BMD_{10}$ or $BMC_{10}$ and $BMDL_{10}$ or $BMCL_{10}$.[123] *In vitro* to *in vivo* extrapolation was performed using an uncertainty factor of 100 based on possible interspecies differences between rodents and humans (10-fold) and interindividual differences (10-fold) in response to a toxicant.[124,125]

## Statistical Analysis

Statistical analysis was performed using GraphPad Prism (version 9; GraphPad Inc.). One-way analysis of variance (ANOVA) was performed for the normality test and homogeneity of variances, followed by Student's *t*-test to compare the numerical data of two treatment groups, including the expression of follicle growth, ovulation related genes between vehicle and 250 μM PFNA-treated follicles, and PFNA accumulation in the whole ovary and follicular fluid. Repeated measurement ANOVA was used to analyze the follicle size measurement data. One-way ANOVA followed by a Tukey's multiple comparison test and Dunnett's adjustment was used to compare numerical data of multiple treatment groups, including the results of follicle diameter, hormone concentration, *in vivo* ovulation and follicle counting, and expression of follicle growth and ovulation related genes. Fisher's exact test was performed to analyze the categorical data of *in vitro* follicle rupture and the first oocyte polar body extrusion. The Cochran-Armitagr test was used to test for trend in PFOA, PFOS, and PFNA. The data was reported as the mean value $\pm$ SD. For the hormone concentration, the measured concentrations were log transformed to address the skewed distribution of the hormonal data and to make the data distribution meet the condition of the parametric statistical analysis for one-way ANOVA between different treatment groups. Statistical significance was defined as a $p < 0.05$.

## Results

### A Tiered *in* Vitro *Ovarian Toxicity Testing in a 3D* in Vitro *Ovarian Follicle Culture System Exposed to PFAS*

We first used our established 3D *in vitro* mouse ovarian follicle culture system, eIVFG, to investigate the ovary-related outcomes and the toxic mechanisms involved following PFAS exposure. We selected three common long-chain PFAS (PFNA, PFOA, and PFOS) and three short-chain PFAS (PFBS, PFHpA, and GenX) that are increasingly used. A tiered toxicity testing pipeline was designed as shown in Figure 1A. In Tier 1, immature mouse follicles were treated with 1–250 μM PFAS during the FSH-stimulated follicle growth window and the hCG-induced ovulation window. Several key follicular events were examined, including follicle development, hormone secretion, ovulation, and oocyte meiosis. PFNA was advanced to Tier 2, in which a specific window of exposure was used to distinguish which follicular functions were perturbed. In Tier 3, more advanced and in-depth molecular
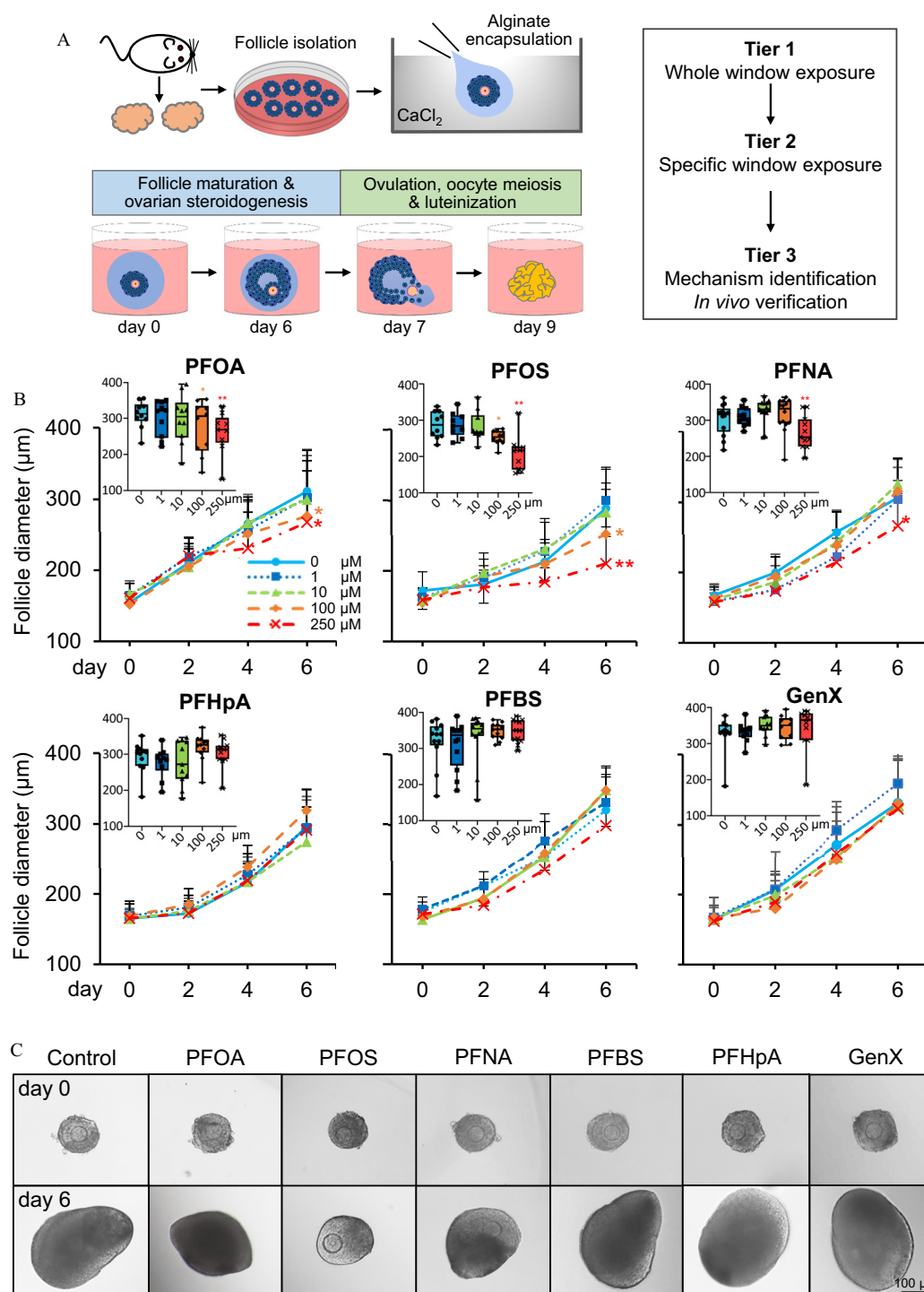
**Figure 1.** A tiered ovarian toxicity testing and the effects of per- and polyfluoroalkyl substances (PFAS) on follicle growth. (A) The schematic of tiered ovarian toxicity testing starting from a 3D eIVFG system. (B) Effects of PFAS on follicle growth. Follicles were treated with either 0.1% DMSO as vehicle control, long-chain (PFOA, PFOS, and PFNA), or short-chain (PFHpA, PFBS, and GenX) at concentrations indicated from day 2. Average follicle diameter on day 6. $n = 10–12$ follicles in each treatment group. Data were analyzed using one-way ANOVA followed by a Tukey's multiple comparisons test. (B) Shown on the line charts are mean ± SD; whiskers above and below box plots indicate the lowest and highest values of data; asterisk indicates the significant difference between different PFAS concentration groups to the control group (vehicle); $^*p < 0.05$ and $^{**}p < 0.01$. (C) Representative follicle images on day 0 and day 6 of eIVFG treated with either vehicle or PFAS at 250 μM, as indicated. Data represented in Figure 1B are included in Excel Table S9. Note: ANOVA, analysis of variance; DMSO, dimethylsulfoxide; eIVFG, encapsulated *in vitro* follicle growth; GenX, ammonium salt of HFPO-DA; hCG, human chorionic gonadotropin; HFPO-DA, hexafluoropropylene oxide dimer acid; PFAS, per- and polyfluoroalkyl substances; PFBA, perfluorobutane sulfonic acid; PFHpA, perfluoroheptanoic acid; PFNA, perfluorononanoic acid; PFOA, perfluorooctanoic acid; PFOS, perfluorooctane sulfonate; SD, standard deviation.

and mechanistic investigations were performed, and verification was conducted in an *in vivo* mouse exposure model.

Tier 1 testing showed that follicles treated with three long-chain PFAS at 1 and 10 μM and three short-chain PFAS at all concentrations during both follicle growth and ovulation windows were able to develop from the secondary stage to the antral stage with comparable size, morphology, and survival on day 6 of eIVFG; however, follicles exposed to 100 and 250 μM
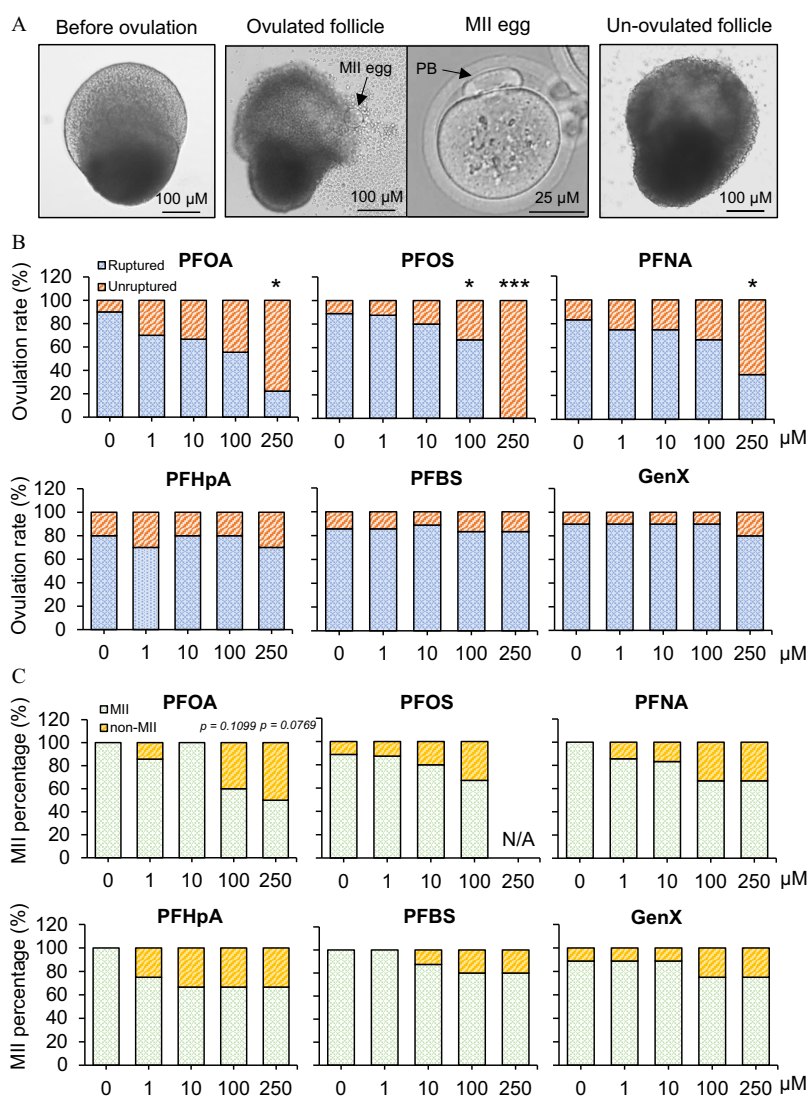
**Figure 2.** Effects of exposure to long-chain and short-chain PFAS during the entire gonadotropin-dependent follicle maturation and ovulation window on follicle ovulation. (A) Representative images of follicles before and after hCG treatment, oocyte with polar body extrusion, and unruptured follicle after PFAS exposure. *In vitro* ovulation was induced by treating follicles with $1.5\,\text{IU/mL}$ of hCG on day 6 of eIVFG for 14 h. (B,C) Percentages of ruptured and unruptured follicles (B) and ovulated MII oocytes (C) treated with various concentrations of long- and short-chain PFAS; $n = 10$ follicles in each treatment group. Statistical analysis was done using Fisher's exact test. Asterisk indicates the significant difference between different PFAS concentration groups to the control group (0 μM); $^{*}p < 0.05$, $^{**}p < 0.01$, and $^{***}p < 0.001$. Data represented in Figure 2A,B are included in Excel Table S10. Note: hCG, human chorionic gonadotropin; eIVFG, encapsulated *in vitro* follicle growth; MII, metaphase II; MII oocytes, oocytes with the first polar body extrusion; PFAS, per- and polyfluoroalkyl substances.

PFOA, or PFOS, or 250 μM PFNA had significantly smaller size (Figures 1B,C). Follicles from day 6 were treated with hCG to induce ovulation. Follicles exposed to each of the three long-chain PFAS demonstrated significantly less percent follicle rupture, a finding that seemed to be concentration related (Figure 2A,B). Follicles treated with PFOA and PFNA at 250 μM and PFOS at 100 μM had significantly reduced percentages of ruptured follicles, and at 250 μM PFOS, no follicle ruptured (Figures 2A,B). Follicles exposed to long-chain PFAS had fewer ovulated MII oocytes, and this finding appeared to be related to concentration, with a decreasing trend (*p* for the trend = 0.0071, 0.001, and 0.0353 for PFOA, PFOS, and PFNA, respectively) and a borderline significance (*p* = 0.0769) for 250 μM PFOA, and no MII oocytes were ovulated from follicles treated with 250 μM PFOS (Figures 2A,C). No significant differences in follicle rupture or oocyte meiosis were identified

for follicles exposed to any of the three short-chain PFAS (Figures 2B,C, lower panels).

Ovarian steroidogenesis was next examined by measuring concentrations of $E_2$ and T in culture media on day 6, corresponding to the end of the follicular phase of an ovarian cycle, and P4 in culture media on day 9, corresponding to the luteal phase. There were no significant differences in hormone secretion between follicles exposed to any of the three short-chain PFAS at any of the tested concentrations (Figure 3). Follicles treated with 250 μM PFOA or PFOS had significantly lower concentrations of $E_2$ (Figure 3A) and T (Figure 3B) on day 6, but they had progesterone secretion comparable to those of the control groups on day 9 (Figure 3C). Secretion of all three hormones was lower after exposure to PFNA at 100 and 250 μM. Although not all were statistically significant, long-chain PFAS, particularly PFNA, at lower concentrations had the tendency to
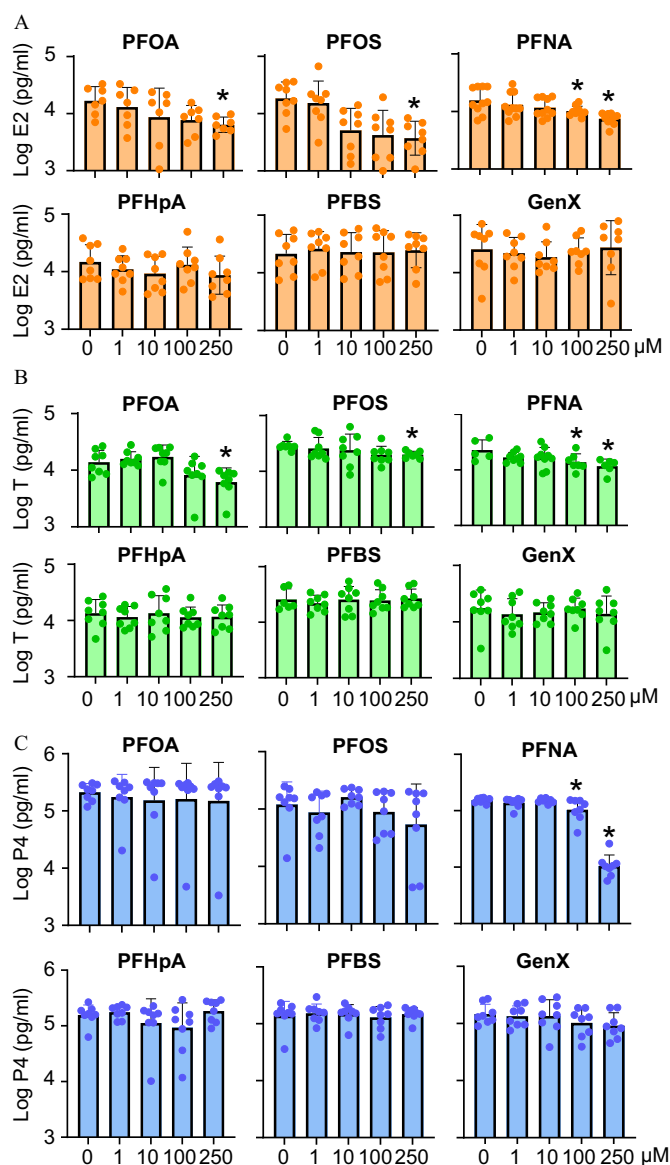
**Figure 3.** Effects of PFAS exposure during the entire gonadotropin-dependent follicle maturation and ovulation window on ovarian steroidogenesis. (A,B) Bars represent the average $\log_{10}$ concentration (pg/mL) of estradiol (A) and testosterone (B) in the conditioned follicle culture media collected on day 6 of eIVFG. (C) Average $\log_{10}$ concentration (pg/mL) of progesterone in the conditioned follicle culture media collected on day 9 after hCG-stimulated follicles were cultured for 48 h. Data were analyzed with one-way ANOVA followed by a Tukey's multiple comparisons test; $n = 5–10$ follicles in each group. Bars represent mean $\pm$ SD; asterisk indicates the significant difference between different PFAS concentration groups to the control group (0 µM); $^*p < 0.05$ and $^{**}p < 0.01$. Data represented in Figure 3A,C are included in Excel Table S11. Note: ANOVA, analysis of variance; eIVFG, encapsulated *in vitro* follicle growth; hCG, human chorionic gonadotropin; PFAS, per- and polyfluoroalkyl substances; SD, standard deviation.

suppress ovarian steroidogenesis in a concentration-dependent manner.

### PFNA Interferes with FSH-Dependent Follicle Growth to Block Ovulation in Vitro

In Tier 2, we used PFNA to perform *in vitro* exposure that was restricted to either the follicle growth window or the ovulation window. Short-chain GenX with the same exposure regimen was used as the negative control.

*FSH-dependent follicle growth, hormone secretion, and follicle morphology after exposure to PFNA in eIVFG.* Follicles were first treated with the same concentration range of PFNA and GenX during the follicle growth window from day 2 to 6 of eIVFG. Consistent with Tier 1, follicles exposed to PFNA but not GenX exhibited significantly smaller follicle diameter (at day 6 in the 250 µM group only), and significantly lower hormonal secretion of $E_2$ and T (at 100 and 250 µM concentrations). Each of these outcomes appeared to be concentration related (Figure S1A). Upon hCG stimulation on day 6, follicles exposed to PFNA at 1, 10, and 100 µM and all concentrations of GenX did not significantly differ from controls in number of follicles rupture and oocyte meiosis on day 7 nor P4 secretion on day 9 (Figure 4A–C). However, those exposed to 250 µM PFNA demonstrated a significantly smaller percentage of ruptured follicles and lower levels of P4 secretion. Percentages of ovulated MII oocytes did not differ from controls (Figure 4A–C).

*Expression of FSH-induced follicle growth genes in eIVFG after exposure to PFNA.* To identify the molecular targets of PFNA during the follicle growth window, we performed a similar exposure experiment by treating follicles with vehicle or 250 µM PFNA from day 2 to 6 of eIVFG. Follicles were collected on day 6 for single-follicle RT-qPCR to examine the expression of several genes crucial for follicle growth. The names, functions, and references of these genes are summarized in Table S3. Results showed that follicles exposed to PFNA had significantly lower expression in comparison with controls of cell proliferation genes *Ccnd2* and *Pcna*, and other genes essential for granulosa cell differentiation and ovarian steroidogenesis, including *Fshr*, *Cyp19a1*, and *Hsd17b1* (Figure 4D). Although not statistically significant, follicles exposed to PFAS had the tendency to have lower expression of several other follicle growth-related genes, including *Pappa*, *Inha*, *Inhba*, *Inhbb*, *Star*, *Cyp11a1*, and *Hsd3b1* (Figure 4D).

*Follicular transcriptome and granulosa cell proliferation and differentiation in eIVFG after exposure to PFNA.* To better understand the effects of PFNA on follicular cell gene expression at the whole transcriptomic level, we collected follicles treated with vehicle or 250 µM PFNA using the same exposure regimen for single-follicle RNA-seq analysis. PCA showed that most PFNA-treated follicles were clearly separated from vehicle-treated follicles (Figure 5A), suggesting a marked alteration of the follicular transcriptome by PFNA exposure. There were 1,004 DEGs with fold change $\geq 2$ or $\leq 0.5$ and FDR $<0.05$, including 337 up- and 667 down-regulated genes in PFNA-treated follicles, with the top 10 genes in each direction highlighted in the volcano plot (Figure 5B). The complete list of all DEGs was deposited in the Gene Expression Omnibus (GSE227267). Most of the gene expression profiles aligned with the RT-qPCR data shown in Figure 4D. The RNA-seq analysis (Figure 5C) also indicated a significantly lower expression of the same set of follicle maturation marker genes, with the exception of *Star* and *Cyp11a1*, which showed higher expression, contrary to the RT-qPCR results.

DEGs were next used for the GO enrichment and KEGG pathway analyses. The specific up-/down-regulated genes for each enriched GO term and signaling pathway are listed in Excel Table S1 and the top 10 GO terms and signaling pathways are highlighted in Figure 5D–G. Biological process analysis revealed that DEGs were primarily enriched in the processes of "Organelle fission" (ratio of up-/down-regulated genes, up/down: 5/76), "Cell cycle" (up/down: 14/159), and "Cytoskeleton organization" (up/down: 14/75) (Figure 5D). Cellular component analysis showed that DEGs were mainly related to "Condensed chromosome centromeric region" (up/down: 1/37), "Kinetochore" (up/down: 1/35), and "Spindle" (up/down: 2/51) (Figure 5E). Molecular function analysis showed that DEGs were closely associated with "Molecular binding" (up/
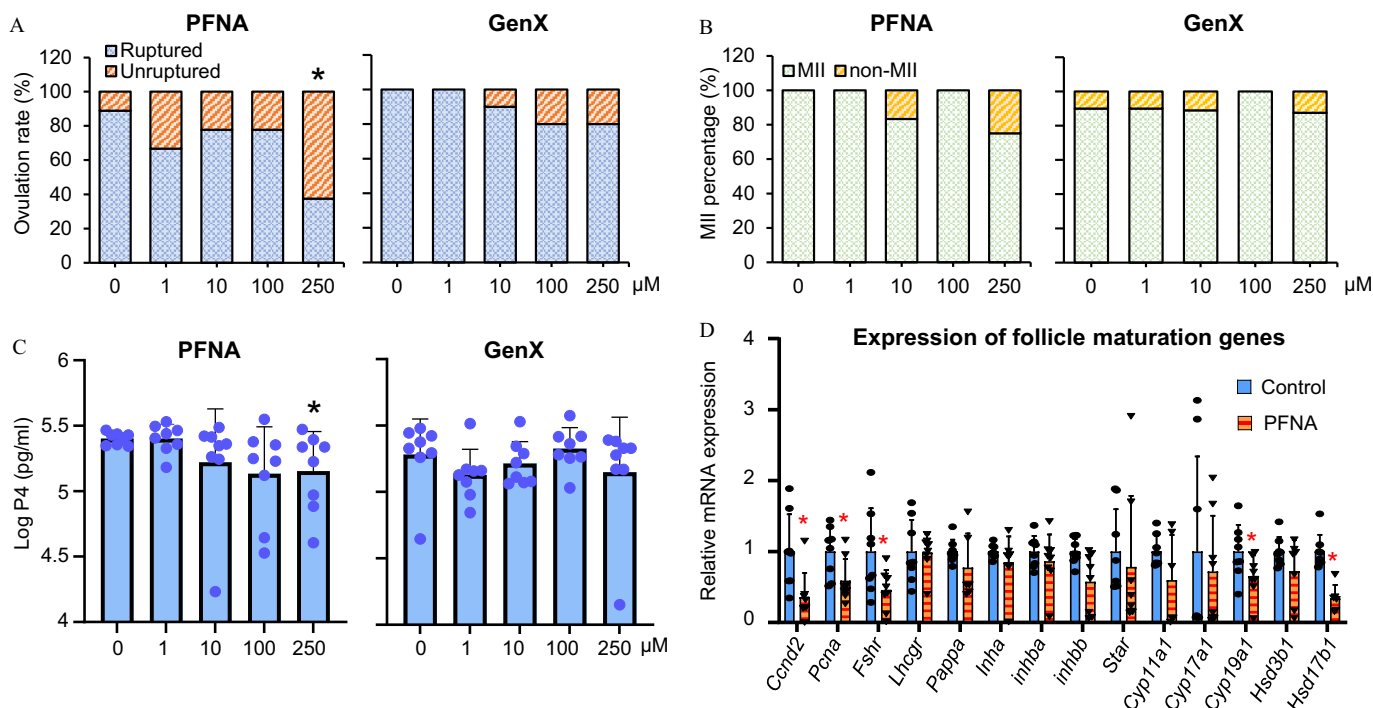
**Figure 4.** Effects of PFNA and GenX on follicle ovulation, resumption of oocyte meiosis, hormone secretion, and expression of follicle maturation genes. Follicles were exposed to various concentrations of PFNA or GenX from day 2 to 6 of eIVFG. (A,B) Percentages of ruptured and unruptured follicles (A) and ovulated MII oocytes (B) treated with various concentrations of PFNA or GenX. (C) Average $\log_{10}$ concentration (picograms per milliliter) of progesterone in the conditioned follicle culture media on day 9 after hCG-stimulated follicles were cultured for 48 h. (D) Relative mRNA expression of follicle maturation genes examined by RT-qPCR in single follicles treated with 250 μM PFNA from day 2 to 6 of eIVFG. The mRNA expression levels were normalized by the expression of *Gapdh*. Data were analyzed with Student's *t*-test. $n = 8–10$ follicles in each group. Shown are mean ± SD; asterisk indicates the significant difference between different PFAS concentration groups in comparison with the control group (0 μM); $^{*}p < 0.05$ and $^{**}p < 0.01$. Data represented in Figure 4A,D are included in Excel Table S12. Note: eIVFG, encapsulated *in vitro* follicle growth; *Gapdh*, glyceraldehyde-3-phosphate dehydrogenase; GenX, ammonium salt of HFPO-DA; hCG, human chorionic gonadotropin; HFPO-DA, hexafluoropropylene oxide dimer acid; MII, metaphase II; MII oocytes, oocytes with the first polar body extrusion; PFAS, per- and polyfluoroalkyl substances; PFNA, perfluorononanoic acid; RT-qPCR, reverse transcription–quantitative polymerase chain reaction; SD, standard deviation.

down: 14/65), "Tubulin binding" (up/down: 6/30), and "ATPase activity" (up/down: 5/35) (Figure 5F). KEGG analysis revealed that several signaling pathways related to cell proliferation and DNA damage response (DDR) were significantly enriched in PFNA-treated follicles, including "DNA replication" (up/down: 0/15), "Cell cycle" (up/down: 1/17), "Mismatch repair" (up/down: 0/6), "Homologous recombination" (up/down: 0/10), and "p53 signaling pathway" (up/down: 2/10) (Figure 5G).

Cell cycle–related genes are shown in the heat map (Figure 5H), and their expression was lower in follicles exposed to PFNA in comparison with control. For instance, 5 out of 6 minichromosome maintenance protein complex (MCM) family genes (*Mcm2-6*), the DNA ligase I gene (*Lig1*), check point kinase 1 gene (*Chek1*), and DNA repair related genes (*Rad51*, *Rad51b*, *Rad54b*, and *Brca1*) were expressed at significantly lower levels in PFNA-treated follicles. We further compared those genes with the predicted PPAR target genes from the PPARgene database[93] via Venn analysis (Figure 5H). There were 30 cell cycle–related genes as well as PPAR target genes, such as *Myc*, *Ccnd2*, and *Cdkn1a*. In addition, the pathways of "Oocyte meiosis" (up/down: 1/17) and "Progesterone-mediated oocyte growth" (up/down: 1/13) were significantly enriched in the KEGG analysis (Figure 5G).

### Follicle Growth and Expression of PPARγ in eIVFG after Exposure to PFNA

To test the hypothesis that PFNA can act as a PPARγ agonist, follicles were coexposed to 250 μM PFNA and various concentrations (0.1, 1, or 10 μM) of PPAR antagonists specifically targeting PPARα, β, or γ during the follicle growth window. Follicles

exposed to any of the three PPAR antagonists alone at all concentrations did not differ from control with regard to follicle growth and ovulation, but those exposed to 250 μM PFNA had consistently less follicle growth and ovulation (Figure 6A,B). PPARγ antagonist (GW9662), but not the PPARα antagonist (MK886) or PPARβ antagonist (GWK3787), rescued the follicle growth and ovulation inhibited by PFNA (Figure 6A,B). At hormone secretion levels, follicles exposed to the antagonist targeting PPARγ but not those targeting PPARα or β, had $E_2$ and T secretion similar to secretion in control follicles on day 6 (Figure 6C). PPARα antagonist (MK886) appeared to rescue $E_2$, but the difference was not statistically significant ($p = 0.6649$). At mRNA expression levels, follicles exposed to PPARγ antagonist (GW9662) and PFNA showed expression of growth-related genes similar to control follicles, including *Fshr*, *Cyp19a1*, *Hsd17b1*, and *Inhbb* (Figure 6D).

### LH/hCG-Dependent Follicle Ovulation in Vitro

To determine whether long-chain PFAS directly affects ovulation per se, similar to the PFAS exposure during the follicle maturation window, we chose PFNA and GenX to treat follicles with the same concentration range and only during the hCG-induced ovulation window. Follicles treated with PFNA at 1 and 10 μM and with GenX at all concentrations had comparable ovulation outcomes on day 7 and P4 secretion on day 9 (Figure 7A–C). However, those exposed to 250 μM PFNA had significantly fewer ruptured follicles, and those exposed to PFNA at 100 and 250 μM had less P4 secretion (Figure 7A,C).
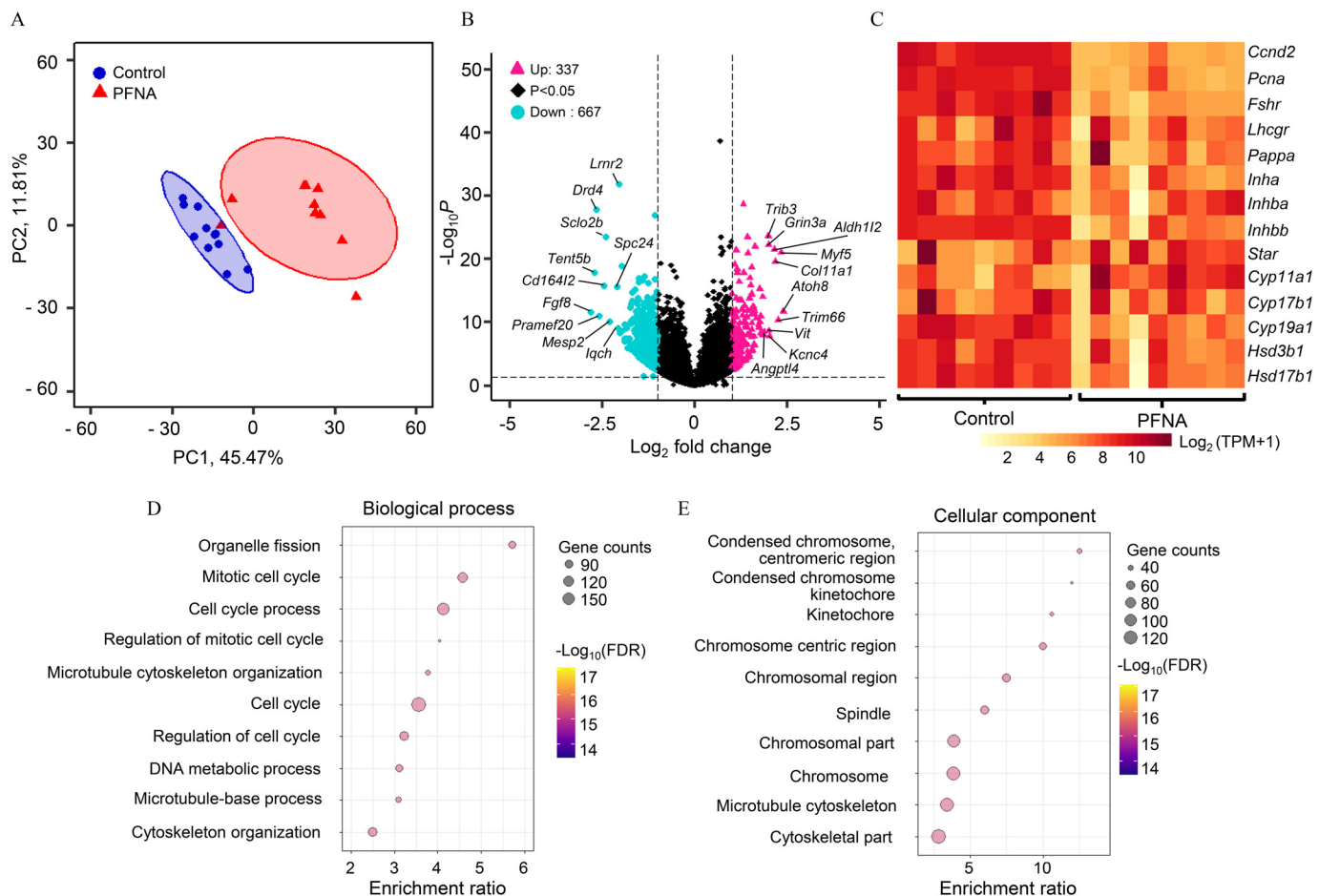
**Figure 5.** Single-follicle RNA-seq analysis of follicles exposed to PFNA during the FSH-stimulated follicle maturation window. (A) PCA of the first two PCs for follicles treated with PFNA at 250 μM ($n = 9$) or vehicle ($n = 10$). (B) Volcano plot of DEGs; FDR <0.05; (absolute fold change ≥2 or ≤0.5) in PFNA-treated follicles in comparison with the control. Pink, red: up-regulated genes; black: insignificantly altered genes; light blue: down-regulated genes. (C) Heat map of the same set of follicle maturation-related genes examined by both single-follicle RNA-seq (here) and RT-qPCR. Each column in the heat map represents the relative difference of expression level in the genes for each sample. GO and KEGG pathway analysis of DEGs identified by single-follicle RNA-seq between follicles treated with PFNA at 250 μM ($n = 9$) or vehicle ($n = 10$) during the follicle maturation window. (D–G) GO analyses of DEGs, including the top 10 enriched biological processes (D), the top 10 enriched cellular components (E), and the top 10 enriched molecular functions (F). (G) Top 10 enriched KEGG pathways. Data represent in Figure 5D–G are also presented in Excel Table S1. (H) Single-follicle RNA-seq data analysis comparing DEGs regulated by PFNA to PPAR target genes during follicle maturation window exposure. Heat map of DEGs in enriched process of "cell cycle" and their comparisons with predicted PPAR target genes from the PPAR gene database. Data represented in Figure 5C are included in Excel Table S13. Note: DEGs, differentially expressed gene; FDR, false discovery rate; FSH, follicle-stimulating hormone; GO, gene ontology; KEGG, Kyoto Encyclopedia of Genes and Genomes; PCA, principal component analysis; PFNA, perfluorononanoic acid; PPAR, peroxisome proliferator–activated receptor; RNA-seq, RNA sequencing; RT-qPCR, reverse transcription–quantitative polymerase chain reaction.

***Expression of key genes involved in follicle rupture and luteinization in eIVFG after exposure to PFNA.*** We collected follicles at 4 h post hCG to examine the expression of several established ovulatory genes using single-follicle RT-qPCR. The names, functions, and related references are summarized in Table S4. Follicles exposed to PFNA had significantly lower expression of key ovulatory genes, including *Pgr*, *Tnfaip6*, *Star*, *Cyp11a1*, *Plau*, and *Il6* (Figure 7D). The lower expression of *Star* and *Cyp11a1*, two genes involved in luteinization and P4 synthesis, is consistent with the lower secretion of P4 in the formed CL organoids (Figure 7C). We collected follicles at 14 h post hCG to examine gelatinase (MMP2/9) activities using *in situ* zymography. In comparison the control group, follicles treated with PFNA had markedly lower GFP fluorescent signals (Figure 7E), indicating decreased gelatinase activation.

***Single-follicle RNA-seq analysis in PFNA-treated follicles.*** To identify molecules responsible for PFNA-associated ovulation defects in an unbiased manner, we collected follicles treated with vehicle or 250 μM PFNA for 4 h for single-follicle RNA-seq analysis. PCA separated vehicle and PFNA-treated follicles into two distinct clusters (Figure 8A), suggesting an altered follicular transcriptome. There were 4,193 significant DEGs with fold change ≥2 or ≤0.5 and FDR <0.05, including 3,103 up- and 1,090 down-regulated genes induced by PFNA during *in vitro* ovulation (Figure 8B). The complete list of all genes is available at the Gene Expression Omnibus (GSE227267). The top 10 genes in each direction are highlighted in the volcano plot in Figure 8B. Consistent with the RT-qPCR data (Figure 8D), the expression of the same set of ovulatory genes was significantly lower in the RNA-seq analysis (Figure 8C).

DEGs were used for GO and KEGG pathway analyses. The specific up-/down-regulated genes for each enriched GO term and signaling pathway are listed in Excel Table S2. Biological process analysis showed that DEGs were primarily enriched in pathways related to "lipid metabolism" (up/down: 156/54), "Angiogenesis" (up/down: 73/40), and "ERK1/2" (up/down: 55/30) (Figure 8D). By comparing with the predicted PPAR target genes from the PPAR gene database, 77 of the 211-lipid metabolism related genes were regulated by PPAR, including *Hmgcs2*, *Cyp27a1*, *Cidea*, and *Slc27a1* (Figure S2A). Molecular function analysis revealed that
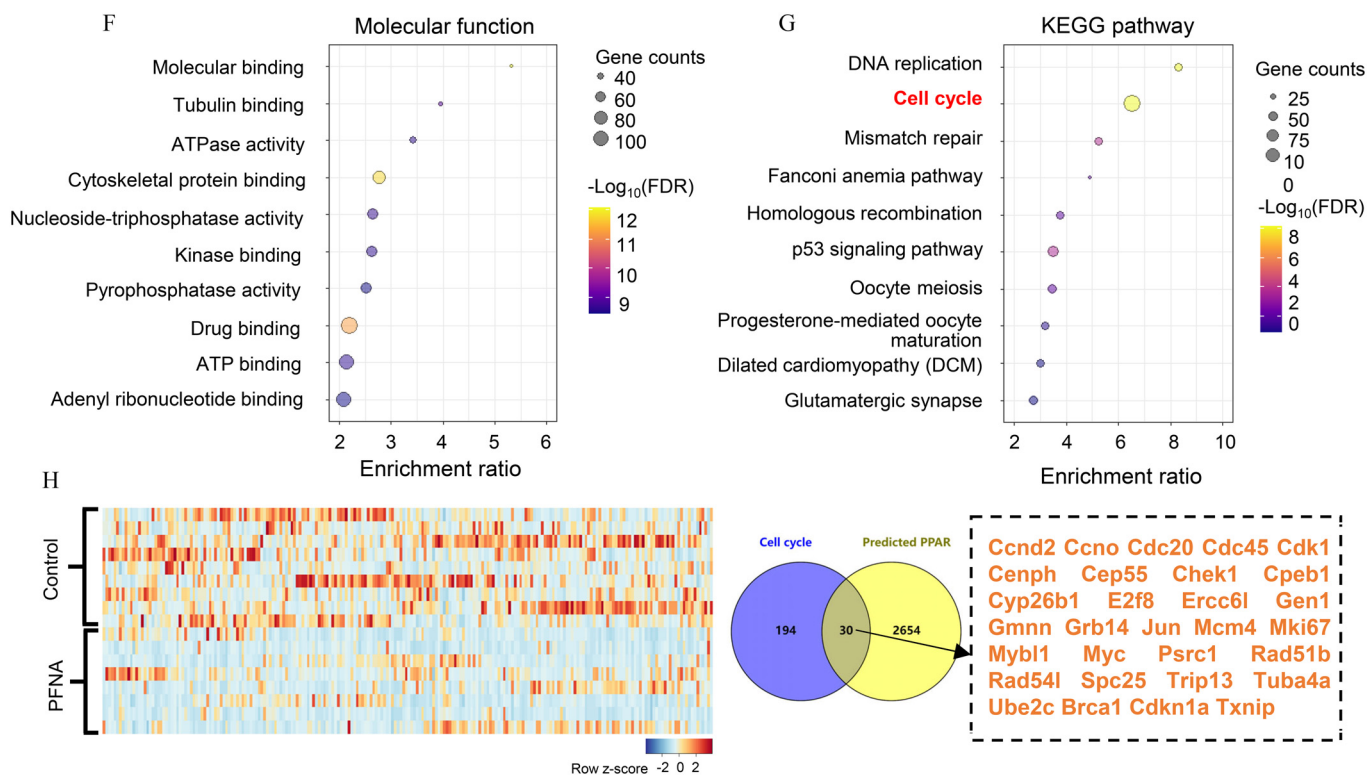
**Figure 5.** (*Continued.*)

DEGs were largely associated with "Ion channel" (up/down: 60/8), "Growth factor activity" (up/down: 33/26), "Calmodulin" (up/down: 59/13), "Actin binding" (up/down: 104/21), and "Catalytic activity" (up/down: 86/36) (Figure 8E). Cellular component analysis showed that DEGs were closely involved in "Extracellular matrix" (up/down: 77/34), "Cell projection" (up/down: 297/87), and "Cell surface" (up/down: 159/92) (Figure 8F). KEGG analysis identified the "Cytokine-cytokine receptor interaction" (up/down: 63/37) as the most significantly altered signaling in PFNA-treated follicles, followed by the "cAMP signaling pathway" (up/down: 66/26), "Calcium signaling pathway" (up/down: 64/18), and "Ovarian steroidogenesis" (up/down: 18/8) (Figure 8G).

Our RNA-seq analysis showed that follicles exposed to PFNA had lower expression of many inflammatory genes, including those encoding cytokines (*Il6*, *Il7*, *Il11*, *Il17a*, *Il33*, *Cxcl2*, *3*, *4*, and *5*), cytokine receptors (*Cxcr4*), and other proinflammatory factors that crucially govern ovulation (*Ptgs1*, *Ptgs2*, and *Tnfaip6*) (Figure 8H). Notably, many of these inflammatory/ovulatory genes have also been established as PPAR target genes, such as *Il1a*, *Il6*, and *Ccl1* (Figure S2B).

We next compared DEGs from PFNA-exposed follicles with another set of DEGs that we previously published at 4 h post hCG in comparison with 0 h in follicles without any xenobiotic treatment in the same *in vitro* ovulation system. There were 1,521 LH/hCG target genes that were consistently different between follicles treated with hCG and PFNA and follicles treated with hCG alone, suggesting adverse impacts of PFNA on the expression of LH/hCG-target genes (Figure S3A; Excel Table S3). However, another 3,921 non-LH/hCG target genes were selectively up- or down-regulated in PFNA-exposed follicles (Figure S3A; Excel Table S4). KEGG pathway analysis revealed that those overlapped LH/hCG target genes were closely related to "Ovarian steroidogenesis," "Peroxisome," and "TNF signaling pathway" (Figure S3B); and the nonoverlapped genes were primarily associated with "Complement and coagulation cascades,"

"Hematopoietic cell linage," and "Aldosterone synthesis and secretion" (Figure S3C).

***Ovulation and ovulatory signaling in PFNA-exposed follicles.*** To investigate whether PFNA activates PPARγ to interfere with ovulation, we first downloaded the gene list of the PPAR pathway from KEGG and the predicted PPAR target genes from the PPAR gene database and performed Gene Set Enrichment analysis (GSEA). The PPAR pathway gene set in PFNA-treated follicles was significantly enriched when compared to that of the control group, with the enrichment score of 0.45, $p = 0.001$, and FDR = 0.002 (Figure 9A). The predicted PPAR target gene set has the enrichment score of 0.22. This gene set was significantly enriched, with a *p*-value of 0.015 and a FDR of 0.171 (Figure 9A). The heat map in Figure 9B also showed that the expression of PPAR-associated genes and signaling in PFNA-treated follicles were significantly different from those of the control.

To further decipher the causation between PFNA-activated PPARγ and ovulation failure, follicles were cotreated with 250 μM PFNA and various concentrations (0, 0.1, 1, and 10 μM) of PPAR antagonists targeting PPARα, β, and γ. Follicles exposed to the PPAR antagonists alone at all concentrations did not differ from control in ovulation (Figure 9C). However, those exposed to PFNA at 250 μM had less follicle rupture (Figure 9C), lower expression of ovulatory genes (Figure 9D), and less P4 secretion (Figure 9E). Follicles cotreated with 10 μM PPARγ antagonist (GW9662) but not the antagonists of PPARα and PPARβ demonstrated a rescued follicle rupture phenotype in comparison with those exposed to PFNA (Figure 9C). Follicles cotreated with the PPARβ antagonist (GSK3787) exhibited a partial rescue effect that did not seem to depend on the concentration of the exposure, but the differences were insignificant in all three concentration groups with *p*-values of 0.0885, 0.1923, and 0.0885 for cotreatment of PFNA with 0.1, 1 and 10 μM GSK3787, respectively (Figure 9C). At both molecular and hormonal levels, a 10 μM PPARγ antagonist (GW9662) rescued
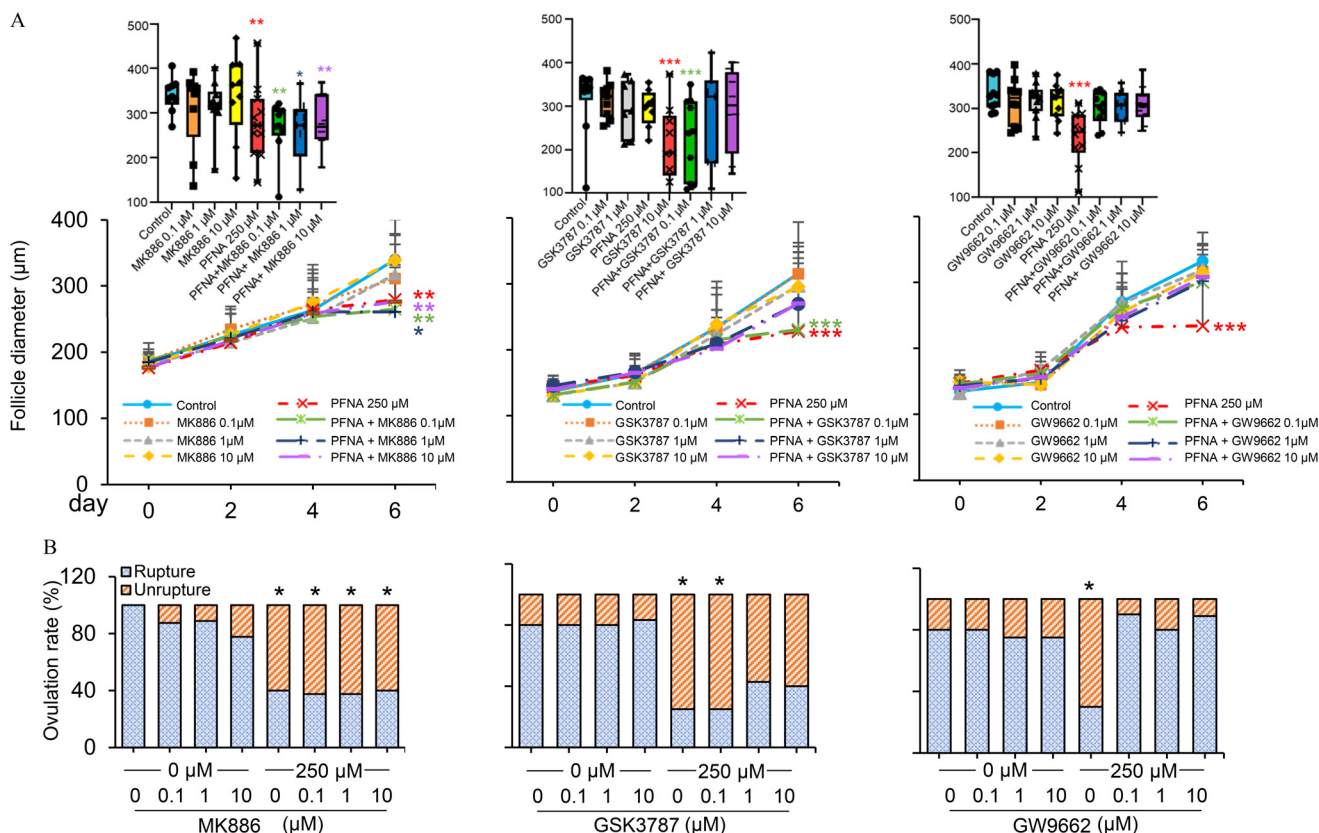
**Figure 6.** The role of PPAR in the effect of PFNA on follicle maturation. (A,B) Follicles were treated with 0, 0.1, 10 μM PPARα antagonist (MK886), PPARβ antagonist (GWK3787), or PPARγ antagonist (GW9662) as indicated, or 250 μM PFNA, or both 0.1–10 μM PPAR antagonists and 250 μM PFNA, or vehicle from day 4 to day 6 of eIVFG. (A) Average diameters of follicles from day 0 to day 6. Insets: Average follicle diameter on day 6. Asterisk indicates the significant difference from different treatment groups to the control group (0 μM); (B) Percentage of ruptured and unruptured follicles; asterisk indicates the significant difference between the cotreatment of PFNA and PPAR antagonist groups to the corresponding PPAR antagonist concentration groups; (C,D) Follicles were treated with 10 μM PPAR antagonists or 250 μM PFNA alone or in combination of both, or vehicle control from day 4–6 of eIVFG. (C) Average $\log_{10}$ concentration of estradiol and testosterone in the conditioned follicle culture media collected on day 6; asterisk indicates the significant difference between two connected groups. (D) Relative mRNA expression of follicle maturation genes examined by RT-qPCR ($n = 8$) in follicles treated with vehicle, 10 μM PPARγ antagonist (GW9662), 250 μM PFNA, or both 10 μM PPARγ antagonist (GW9662) and 250 μM PFNA; asterisk indicates the indicate significant difference between two connected groups. Expression levels were normalized by the expression of *Gapdh*. Data were analyzed with Student's *t*-test (A), Fisher's exact test (B), and one-way ANOVA followed by a Tukey's multiple comparisons test (C,D), $n = 8$–10 follicles in each treatment group. Shown are mean ± SD. Data represented in Figure 6 are included in Excel Table S14. Note: ANOVA, analysis of variance; eIVFG, encapsulated *in vitro* follicle growth; *Gapdh*, glyceraldehyde-3-phosphate dehydrogenase; PFNA, perfluorononanoic acid; PPAR, peroxisome proliferator–activated receptor; PPARα, peroxisome proliferator–activated receptor alpha; PPARβ, peroxisome proliferator–activated receptor lowercase beta; PPARγ, peroxisome proliferator–activated receptor lowercase gamma; RT-qPCR, reverse transcription–quantitative polymerase chain reaction; SD, standard deviation. *$p < 0.05$; **$p < 0.01$; and ***$p < 0.001$.

the expression of key ovulatory genes inhibited by PFNA, including *Star*, *Cyp11a1*, *Plau*, and *Il6* (Figure 9D) as well as P4 secretion in PFNA-treated follicles (Figure 9E).

### Follicle Development and Ovulation in Vivo after Exposure to PFNA

We next used an *in vivo* mouse model of acute PFNA exposure to verify the outcomes observed in the *in vitro* follicle culture system above as well as measure the ovarian accumulation of PFNA upon *in vivo* exposure. As shown in Figure 10A, 21-d-old prepubertal CD-1 female mice were treated with vehicle or 1, 5, and 25 mg/kg PFNA via IP injection for 5 d, with PMSG and hCG injections on day 3 and 5, respectively, to induce superovulation. PFNA-exposed mice had significantly fewer ovulated oocytes retrieved from both sides of oviducts in comparison with the control group, with $20.33 \pm 11.45$, $11.23 \pm 8.22$, and zero ovulated oocytes in mice treated with 1, 5, and 25 mg/kg PFNA, respectively, in comparison with $23.44 \pm 11.14$ oocytes in the control group (Figure 10B). This appeared to be dose dependent. Ovarian histology and follicle counting results confirmed

significantly more unruptured late-staged antral follicles in mice treated with 25 mg/kg PFNA ($7.67 \pm 2.16$ in vehicle vs. $22.17 \pm 2.40$ PFNA-treated mice; Figure 10C,D).

The analytical results of UHPLC-HRMS showed that PFNA was nondetectable in the serum, ovary, or follicular fluid of vehicle-treated mice, indicating negligible background contamination (Figure 10E; Figure S4). In mice treated with 1, 5, and 25 mg/kg PFNA, the serum concentrations of PFNA were $5.1 \pm 0.9$, $19.3 \pm 1.7$, and $250.6 \pm 97.8$ μg/mL, respectively; the amounts of PFNA in the whole ovary were $1.6 \pm 0.6$, $7.9 \pm 2.2$, and $130.7 \pm 25.1$ ng per ovary, respectively; and the amounts of PFNA in the follicular fluid of large antral follicles were $1.2 \pm 0.4$, $5.1 \pm 2.5$, and $22.1 \pm 3.1$ ng per ovary (Figure 10E; Table S5). Based on the estimation that $\sim 20$ large antral follicles were sampled in each ovary to collect the follicular fluid, and a large antral follicle has an average volume of $0.019\ \text{mm}^3$ or μL (Figure S5), the PFNA concentrations in the follicular fluid were estimated to be 6.7, 28.8, and 125.9 μM in mice treated with 1, 5, and 25 mg/kg PFNA, respectively, which are within the range of PFAS concentrations in women's systemic circulation or follicular fluid (1 nM–222 μM) reported in previous studies.[20,25–36,83]
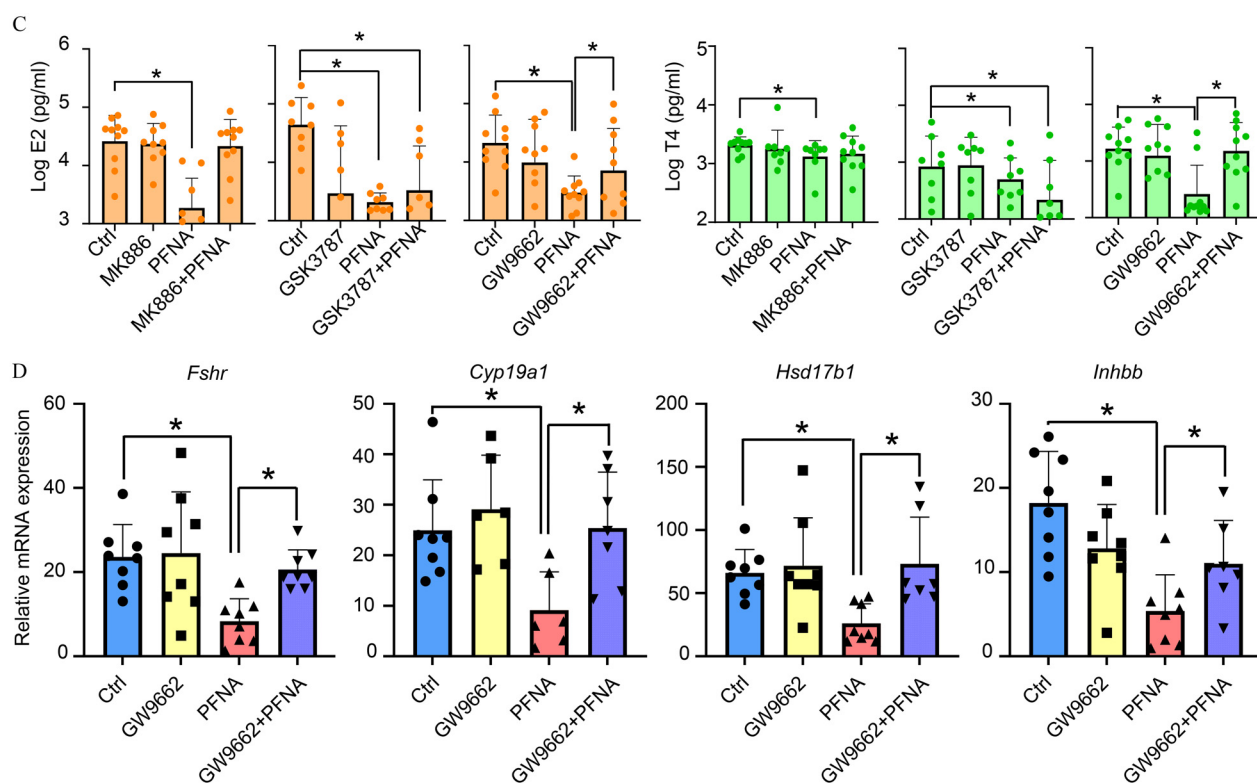
**Figure 6.** (*Continued.*)

Moreover, as found in humans, the PFNA FF: serum partition coefficient in mice exposed to 1 or 5 mg/kg PFNA is 0.61 or 0.69, respectively (Table S5). At higher dose of 25 mg/kg, the coefficient dropped to 0.23.

We next collected follicular somatic cells from large antral follicles in the ovaries of PBS- or 1, 5, and 25 mg/kg PFNA-treated mice at 4 h post hCG injection for RT-qPCR and *in situ* RNA hybridization. In comparison with the control group, PFNA-exposed follicles had lower expression of ovulatory genes, including *Star*, *Pgr*, *Ptgs2*, *Tnfaip6*, *Adamts1*, *Plat*, *Plau*, and *Il6* (Figure 10F). There was no significant difference in other hormone secretion related genes, such as *Cyp11a1*, *Cyp17b1*, and *Cyp19a1*, or ovulatory genes encoding factor EGF-like factors, such as *Areg*, *Ereg*, and *Btc* (Figure S6). *In situ* RNA hybridization results confirmed the lower expression of *Star*, *Ptgs2*, and *Tnfaip6* in follicular theca and/or granulosa cells in the ovaries of 25 mg/kg PFNA-treated mice (Figure 10G).

To verify the mechanistic role of PPARγ in PFNA-induced defective follicle growth and ovulation observed *in vitro*, 21-d-old prepubertal CD-1 female mice were treated with vehicle, 25 mg/kg PFNA, 1 mg/kg PPARγ antagonist (GW9662), or both PPARγ antagonist (GW9662) and PFNA during PMSG/hCG-induced superovulation. Mice treated with vehicle or PPARγ antagonist (GW9662) alone had comparable numbers of ovulated oocytes ($30.38 \pm 8.12$ in control vs. $27.80 \pm 3.28$ PPARγ antagonist (GW9662)-treated mice; Figure 10H). Those exposed to 25 mg/kg PFNA alone had fewer oocytes; however, the cotreatment with PPARγ antagonist (GW9662) and PFNA resulted in significantly more ovulated oocytes ($15.44 \pm 12.42$ in cotreatment vs. zero in PFNA alone; Figure 10H).

### BMD Modeling for *in Vitro and* in Vivo *End Points*

For the *in vitro* dual-window exposure (growth and ovulation) experiments, the $BMC_{10}$ and $BMCL_{10}$ of end points that were significantly different after exposure to PFAS are presented respectively in Excel Table S5–S7, for continuous end points including follicle diameter, $E_2$, T, and P4 secretion, and for dichotomous end points of follicle rupture and oocyte meiotic resumption. The $BMC_{10}$ values ranged widely, between 2 and 2,000 μM, whereas the $BMCL_{10}$ values ranged between 1 and 160 μM. Extrapolating these values using an uncertainty factor of 100 for the *in vitro* to *in vivo* extrapolation suggests reference concentrations of 10 nM–1.60 μM for a 10% extra risk of follicular defects in humans. The $BMCL_{10}$ values for the long-chain PFOA, PFOS, and PFNA generally extended to a low concentration of 0.998 μM. The follicle rupture seemed to be a more sensitive end point than hormone secretion and follicle growth, especially for the three long-chain PFAS, with $BMCL_{10}$ at 5.7, 0.998, and 4.95 μM for PFOA, PFOS, and PFNA, respectively (Excel Table S5). An interesting finding was that when the BMD analysis was applied to the distinct window exposure experiments for PFNA, the $BMCL_{10}$ for inhibition of follicle rupture was lower when the exposure was limited to the growth window (10.37 μM) than when it was limited to the ovulation window (28.83 μM) (Figure 11A; Excel Table S6). Moreover, the $BMCL_{10}$ of the dual-window exposure was 4.95 μM. In comparison, the oocyte meiosis I resumption did not seem to be sensitive to the exposure of either single or dual windows (Figure 11B).

For the *in vivo* superovulation experiment, the $BMD_{10}/BMC_{10}$ and $BMDL_{10}/BMCL_{10}$ of PFNA for blocking ovulation were 3.2 mg/kg (32.5 μM in serum, 20.2 μM in FF) and 1.4 mg/kg (16.6 μM in serum, 10.6 μM in FF), respectively (Excel Table S7). Moreover, the $BMC_{10}$ and $BMCL_{10}$ of PFNA for inhibiting ovulatory genes, such as *Star*, *Pgr*, and *Ptgs2*, were 4.3–34.7 μM and 1.7–11.2 μM in serum, respectively (Excel Table S7). In mice treated with 1 mg/kg PFNA, the dose close to the calculated $BMDL_{10}$ of 1.4 mg/kg, the analytical results of UHPLC-HRMS showed that the accumulation levels of PFNA were $11.0 \pm 1.9$ μM, 1.6 ng/ovary, and $6.7 \pm 2.2$ μM in the serum, homogenized ovary,
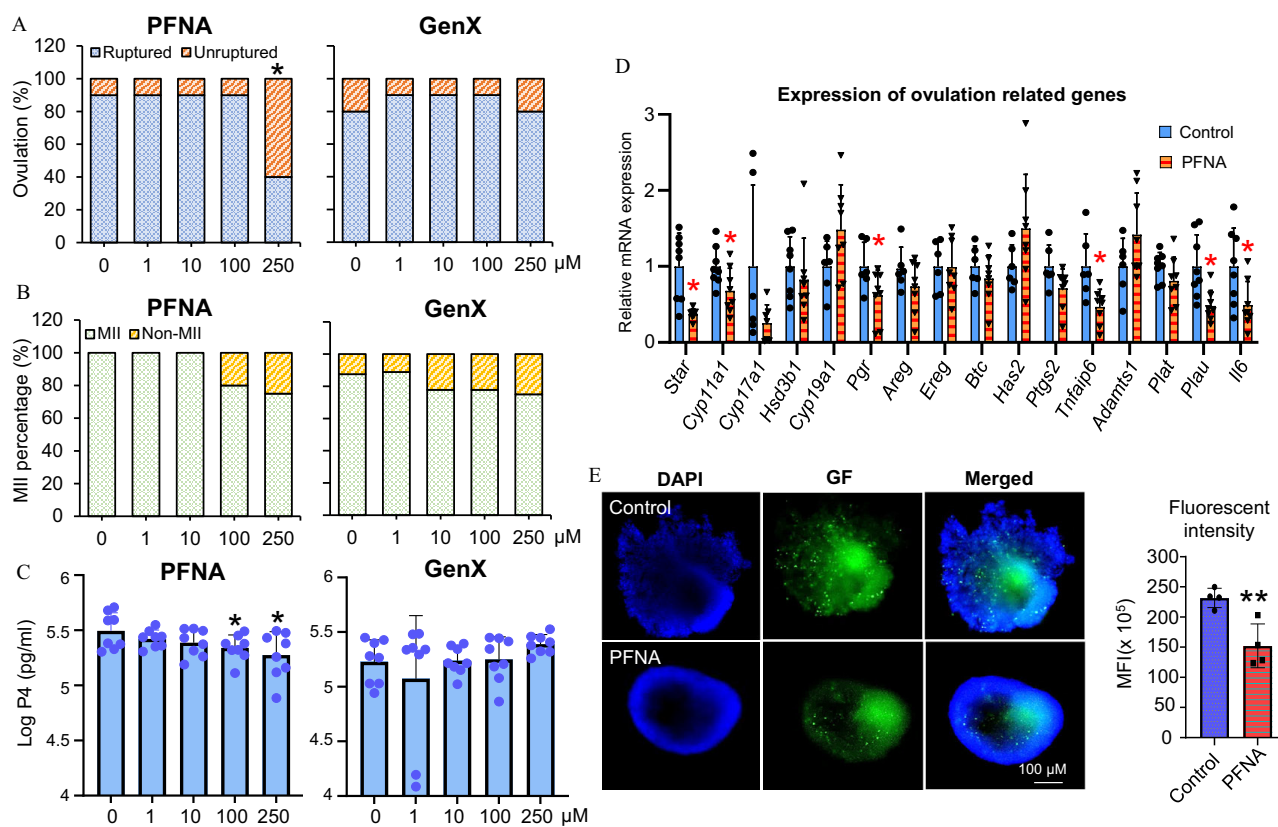
**Figure 7.** Effects of PFNA and GenX on follicle ovulation, expression of ovulatory genes, and gelatinase activity. Follicles were exposed to various concentrations of vehicle, PFNA, or GenX as well as 1.5 IU/mL hCG on day 6 of eIVFG for *in vitro* ovulation induction. (A) Percentages of ruptured and unruptured follicles treated with various concentrations of PFNA and GenX. (B) Percentage of ovulated MII oocytes. (C) Average $\log_{10}$ concentration (pg/mL) of progesterone in the conditioned follicle culture media after hCG-stimulated follicles were cultured for 48 h ($n = 8$). (D) Relative mRNA expression of ovulation-related genes at 4 h of post-hCG treatment was examined by RT-qPCR. Expression data were normalized with the expression of *Gapdh*. (E) Representative images and quantification of *in situ* zymography of follicles treated with vehicle or PFNA at 14 h post hCG. Data were analyzed with Fisher's exact test (A,B), and Student's *t*-test (C–E). Shown bars represent mean ± SD; $n = 8–10$ follicles in each treatment group; asterisk indicates the significant difference from different treatment groups to the control group (0 μM); *$p < 0.05$; **$p < 0.01$. Data represented in Figure 7 are included in Excel Table S15. Note: eIVFG, encapsulated *in vitro* follicle growth; *Gapdh*, glyceraldehyde-3-phosphate dehydrogenase; GenX, ammonium salt of HFPO-DA; hCG, human chorionic gonadotropin; HFPO-DA, hexafluoropropylene oxide dimer acid; MFI, mean fluorescent intensity; MII, metaphase II; MII oocytes, oocytes with the first polar body extrusion; PFNA, perfluorononanoic acid; RT-qPCR, reverse transcription–quantitative polymerase chain reaction; SD, standard deviation.

and follicular fluid of large antral follicles, respectively (Excel Table S7; Figure 10E).

## Discussion

Approximately 10%–15% of women of reproductive age experience reproductive disorders and infertility, with ovarian disorders as the leading cause.[126–128] The etiology of these ovarian dysfunctions remains elusive but has been related to exposure to environmental endocrine-disrupting chemicals,[129] including PFAS.[130] Many countries globally have implemented laws and policies to reduce PFAS pollution and exposure. However, due to the high persistence and long half-lives, the long-chain legacy PFAS remains prevalent; moreover, the female reproductive impact of other long-chain PFAS, such as PFNA, and emerging short-chain alternatives, such as GenX, is largely unknown. Here, our findings using a 3D *in vitro* ovarian follicle culture system and an *in vivo* mouse model suggest that exposure to long-chain PFAS interfered with gonadotropin-dependent follicle growth, ovulation, and hormone secretion; in addition, PFNA, an understudied long-chain PFAS that has been reported to reach similar or even higher contamination levels than the legacy PFOA and PFOS in some community water bodies,[131,132] activated PPARγ (as shown by higher expression of downstream genes) in granulosa cells, suggesting this as the MIE for the aforementioned ovarian outcomes.

Both of our *in vitro* and *in vivo* results suggest that long-chain PFAS interfered with ovulation. Through two distinct *in vitro* PFNA exposures and in-depth analysis using eIVFG, we further demonstrated that long-chain PFAS, particularly PFNA, perturbed both gonadotropin-dependent follicle growth and ovulation. During FSH-stimulated follicle growth, follicles exposed to PFNA exhibited delayed follicle growth and less hormonal secretion of $E_2$ and T. In line with these morphological and hormonal changes, molecular analysis using RT-qPCR and RNA-seq revealed that exposed follicles had lower expression of key genes regulating cell cycle and granulosa cell proliferation (*Ccnd2* and *Pcna*), ovarian steroidogenesis (*Cyp19a1*, *Hsd3b1*, and *Hsd17b1*), and follicle growth (*Fshr*). When mature follicles were exposed to PFNA only during the ovulation window, they had less follicle rupture and lower P4 secretion. Our results further revealed that, despite minor discrepancies between RT-qPCR and RNA-seq data, the overall RNA-seq findings support the hypothesis that PFNA suppresses the expression of FSH target genes, disrupting follicle maturation and other follicle/oocyte reproductive outcomes. Moreover, exposed follicles had lower expression of key ovulatory genes involved in extracellular matrix (ECM) remodeling (*Pgr*, *Plau*, and *Adamts1*), cumulus expansion (*Has2* and *Tnfaip6*), inflammation (*Il6*, *Cxcl2*, and *Ptgs2*), and luteal steroidogenesis (*Star*, *Cyp11a1*, and *Hsd3b1*). These findings suggest that long-chain PFAS also directly affect
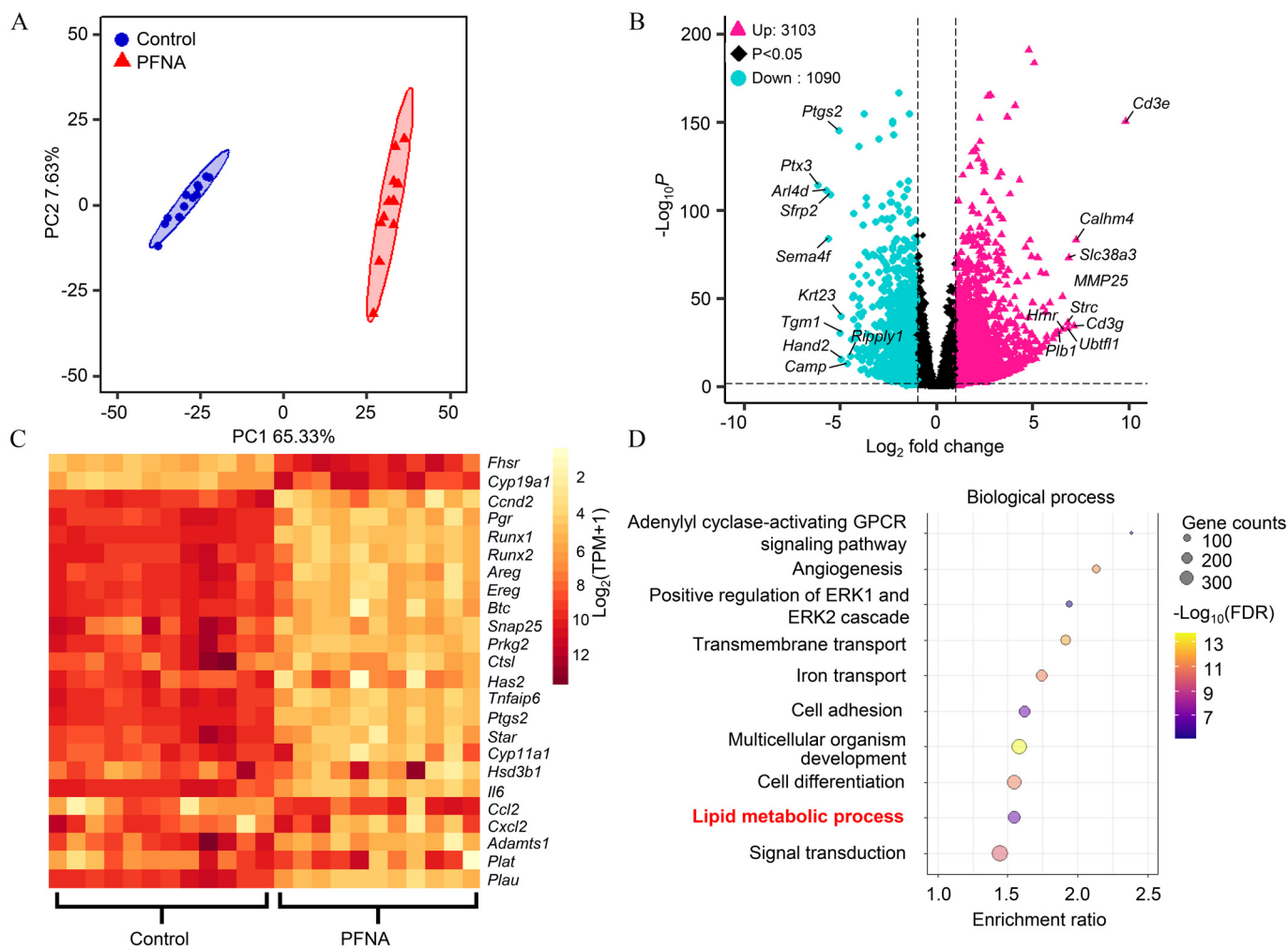
**Figure 8.** Single-follicle RNA-seq analysis of follicles exposed to PFNA during the ovulation window only. (A–H) Follicles were treated with vehicle control or 250 μM PFNA and 1.5 UI/mL hCG for 4 h on day 8 of eIVFG. (A) PCA of the first two principal components for follicles treated with PFNA ($n = 10$) or vehicle control ($n = 11$). (B) Volcano plot of differentially expressed genes (DEGs; FDR <0.05; absolute fold change >2 or < − 2) in PFNA-treated follicles in comparison with the control group. Pink, red: up-regulated genes; black: nonsignificantly altered genes; light blue: down-regulated genes. (C) Heat map indicating relative change of ovulatory genes in PFNA-treated follicles (column 12–21) and control (column 1–11). (D,F) GO analyses of DEGs, including the top 10 biological process enrichment results (D), the top 10 cellular component enrichment results (E), and the top 10 molecular function enrichment results (F). (G) Top 10 KEGG pathway enrichment results. (H) Heat map indicating relative change of inflammatory genes in PFNA-treated follicles (column 12–21) and control (column 1–11). Data presented in Figure 8C,H are included in Excel Table S16; Figure 8D,G data are included in Excel Table S2. Note: DEG, differentially expressed gene; eIVFG, encapsulated *in vitro* follicle growth; FDR, false discovery rate; GO, gene ontology; hCG, human chorionic gonadotrophin; KEGG, Kyoto Encyclopedia of Genes and Genomes; PCA, principal component analysis; PFNA, perfluorononanoic acid; RNA-seq, RNA sequencing.

ovulation per se (Excel Table S8). As demonstrated by the BMD modeling analysis, when both the growth and ovulation windows were perturbed by PFNA, the $BMCL_{10}$ became much lower, suggesting that PFNA may act on the two processes synergistically to disrupt ovulation.

For both *in vitro* and *in vivo* exposure studies, our goal was to test multiple high and low concentrations/doses of PFAS to obtain concentration–response or dose–response curves, such that we could estimate the PoD concentration/dose, which are routinely used in chemical risk assessment. We used $BMCL_{10}$, which takes assay uncertainty into consideration, to estimate the PoDs[133] and compared them with the internal exposure levels in humans. When comparing the $BMCL_{10}$ of the most sensitive end point of follicle rupture (5.7, 0.998, and 4.95 μM for PFOA, PFOS, and PFNA, respectively) with the highest follicular fluid concentrations available in women in the general population (1.44, 0.362, and 0.008 μM for PFOA, PFOS, and PFNA, respectively),[31] the equivalent bioactivity exposure ratios (BER), which are a margin of safety (MoS) metric for risk assessment using *in vitro* data,[134]

are $5.7/1.44 = 3.95$, $0.998/0.362 = 2.76$, and $4.95/0.008 = 618$, respectively. However, given that PFAS concentrations in follicular fluid are expected to be comparable to or only slightly lower than serum concentrations, as we described in the "Materials and Methods" section, using the highest serum PFAS concentrations in humans as an approximate surrogate, which are 222 μM,[33] 25.6 μM,[32] and 0.086 μM[25] (Table S1), the corresponding BERs are $5.7/222 = 0.025$, $0.998/25.6 = 0.04$, and $4.95/0.086 = 57.6$ for PFOA, PFOS, and PFNA, respectively. The lower the BER or MoS, the higher the risk. Therefore, our results suggest that PFOA and PFOS posed much higher risks than PFNA. However, as an emerging guideline for uncertainty consideration when using *in vitro* assays for next generation risk assessment, even BER <100 may not be adequate to account for the uncertainties inherent in the *in vitro* approach.[135,136] Because we are not using human cells or tissues here, there is additional interspecies uncertainty. Therefore, with a BER of 57.6, PFNA may pose a nonnegligible risk of ovarian adverse outcomes, which requires further investigation. For the *in vivo* exposure data, when comparing the $BMCL_{10}$
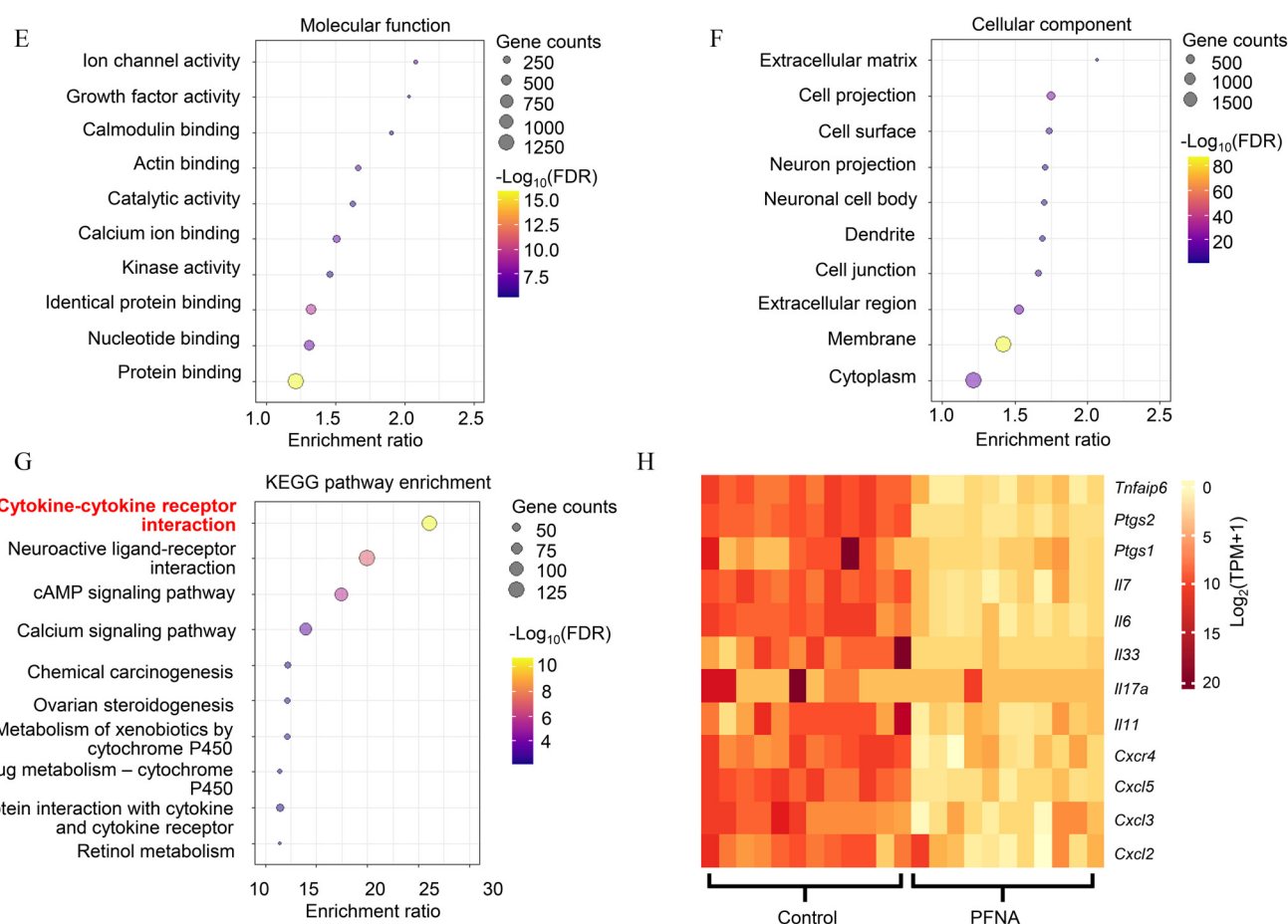
**Figure 8.** (*Continued.*)

of 16.6 μM for inhibiting follicle rupture and 1.7–11.2 μM for suppressing ovulatory genes, the MoS were $16.6/0.086 = 193$ and between $1.7/0.086$ and $11.2/0.086 = 19.8$–130, respectively. Even at 193 or 130, the MoS values are borderline cases, suggesting the PFNA levels in some individuals may pose a nonnegligible risk of ovarian adverse outcomes. It is notable that the PFNA FF:serum partition coefficient in mice exposed to lower concentration of PFNA (1 or 5 mg/kg) was stable at around 0.6, which indicated the high PFNA distribution and bioaccumulation in follicular fluid from serum; whereas at a higher dose of PFNA, the coefficient dropped potently, suggesting that the follicular uptake of PFNA may be membrane transporter–mediated and is saturated at high concentrations, as has been observed in other tissues.[137,138]

Accumulating evidence reveals that PFAS, particularly long-chain PFAS, can act as a PPAR agonist to exhibit toxicities, including endocrine-disrupting effects.[69,70] PPARs heterodimerize with 9-cis-retinoic acid receptors (RXRs) to form the PPAR/RXR heterodimer, which binds to the PPAR response element (PPRE) in the promoter region of PPAR target genes to regulate their transcription.[139] PPARs are involved in various physiological and pathophysiological processes, including lipid metabolism, anti-inflammatory effects, and suppression of cell proliferation.[140,141] For the three PPAR subtypes, PPARα and β are expressed in the ovarian stromal and theca cells, and their expression levels are stable through folliculogenesis and ovulation; whereas PPARγ is primarily expressed in the outer layered mural granulosa cells of maturing follicles and is down-regulated in preovulatory follicles and ovulating follicles.[71–74] Although the exact functions of PPARs in the ovary are not fully understood, PPARγ has been shown to regulate sheep granulosa cell proliferation, ovarian steroidogenesis in mice, and tissue remodeling.[142] In maturing follicles, the overactivation of PPARγ by synthetic agonists (e.g., troglitazone) has been found to inhibit proliferation of granulosa cells from sheep and cattles,[71,74] aromatase expression in human granulosa cells,[143–145] and $E_2$ secretion in sheep, mouse, rat, cattle, and human.[71,72,74,143–147] PPARγ has also been suggested as a transcriptional repressor to suppress overexpression of LH-target genes, which prevents premature luteinization of granulosa cells.[75,76] Our RNA-seq analysis revealed that follicles exposed to PFNA during growth had lower expression of genes related to cell cycle, and many of these cell cycle–related genes are PPAR target genes; moreover, PFNA-treated follicles had significantly higher expression of several LH-target genes, such as *Areg*, *Ereg*, *Pgr*, *Runx1/2*, *Il6*, and *Cxcl1* (Figure S8). Ovulation has been proven to be an inflammatory process.[148] LH stimulates the expression of proinflammatory factors at the early stage of ovulation, such as cytokines and prostaglandins, to promote immune cell attraction, proteolysis, ECM remodeling, and angiogenesis.[149,150] In response to the LH surge, the downregulation of the abundance and activity of PPARγ is obligatory for the induction of cytokines and other inflammatory factors to induce ovulation.[151] As a key regulator of lipid metabolism, the activation of PPARγ has also been related to the hormone and energy imbalance during ovulation as well as oocyte maturation.[144,152–155] Our RNA-seq data using PFNA-treated ovulating follicles revealed that follicles exposed to PFNA had lower expression of key inflammatory genes and higher expression of genes related to lipid metabolism.
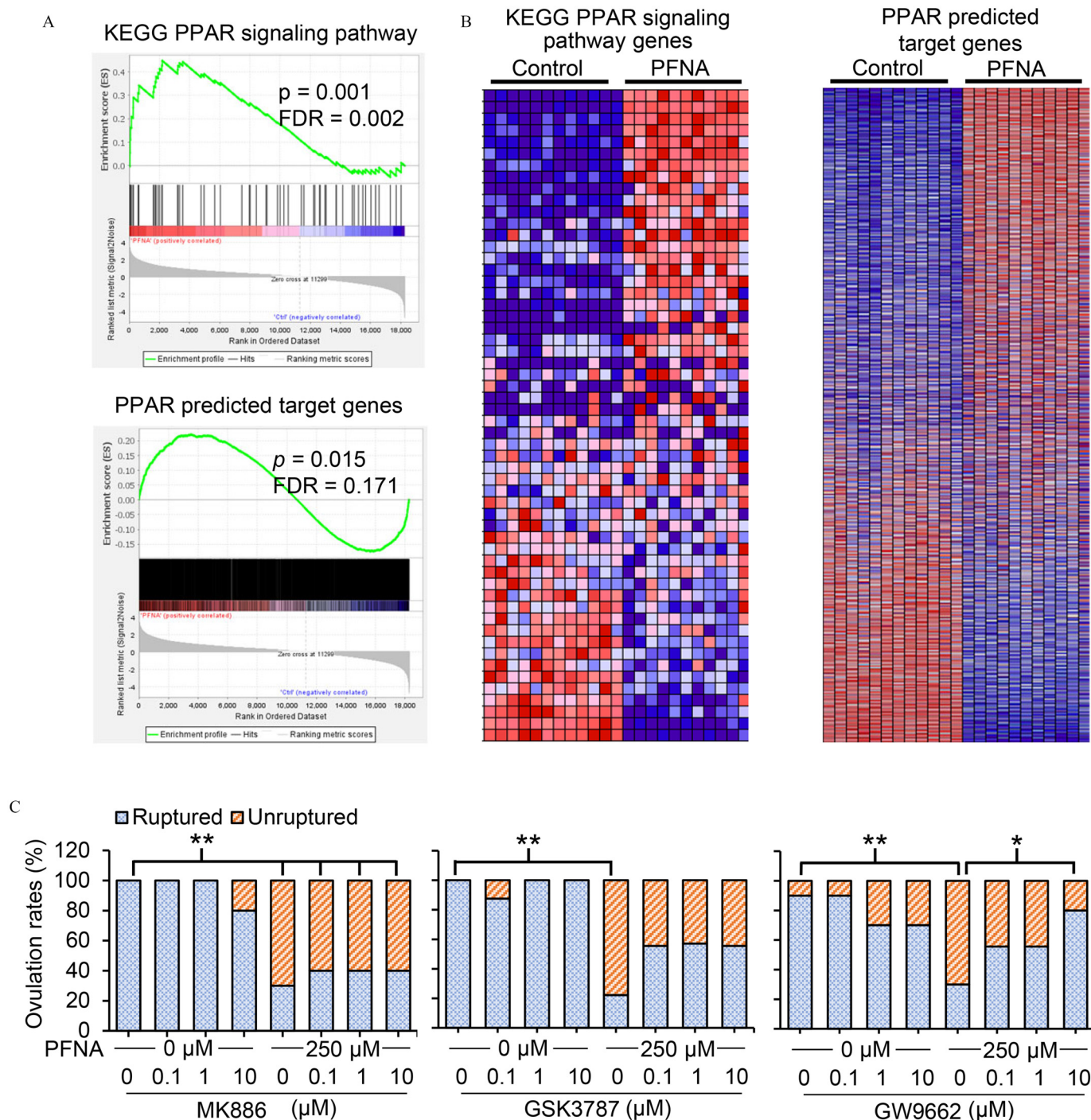
**Figure 9.** The role of PPAR in the effect of PFNA on follicle ovulation. (A) GSEA of DEGs, including KEGG PPAR signaling pathway gene sets and predicted PPAR target genes. (B) Heat map of genes in the KEGG PPAR signaling pathway and predicted PPAR target genes. Columns represent the relative difference of expression level of genes in each sample. (C) Follicles were treated with 0, 0.1, 1, 10 μM PPAR antagonists, or 250 μM PFNA, or combination of PPAR antagonists and PFNA, or vehicle control. Follicle rupture was then examined at 14 h post hCG and ($n = 10$); asterisk indicates the significant difference between the cotreatment of PFNA and PPAR antagonist groups to the corresponding PPAR antagonist concentration groups. (D) Relative mRNA expression of ovulatory genes examined by RT-qPCR; follicles were treated with 10 μM PPARγ antagonist (GW9662), 250 μM PFNA, or a combination of both, or vehicle control with hCG for 4 h ($n = 8$). The expression level of each gene was normalized by the expression of *Gapdh*. Asterisk indicates the significant difference between two connected groups. (E) Average $\log_{10}$ concentration of progesterone in conditioned ovulation-induction media collected 48 h post hCG ($n = 8-10$); asterisk indicates the significant difference between two connected groups. Statistical analyses were done with Fisher's exact test (B) and one-way ANOVA followed by a Tukey's multiple comparisons test (C,D). Bars represent mean ± SD. Data presented in Figure 9 are presented in Excel Table S17–S18. Note: ANOVA, analysis of variance; *Gapdh*, glyceraldehyde-3-phosphate dehydrogenase; GSEA, gene set enrichment analysis; hCG, human chorionic gonadotrophin; KEGG, Kyoto Encyclopedia of Genes and Genomes; PFNA, perfluorononanoic acid; PPAR, peroxisome proliferator–activated receptor; RT-qPCR, reverse transcription–quantitative polymerase chain reaction; SD, standard deviation. $^*p < 0.05$; $^{**}p < 0.01$; and $^{***}p < 0.001$.
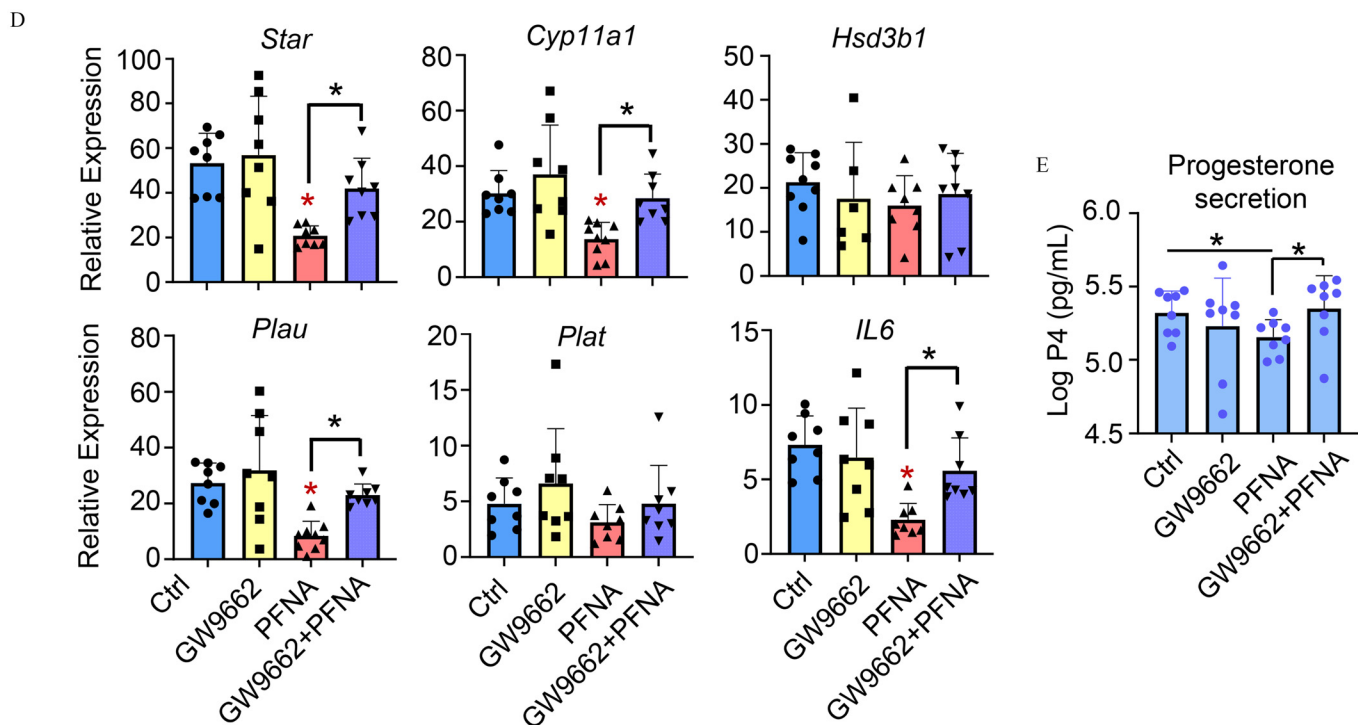
D



E



**Figure 9.** (*Continued.*)

The results and discussion above support our hypothesis that in mice, PPARγ is the molecular target of PFNA, and exposure to PFNA may disrupt granulosa cell differentiation in maturing and ovulating follicles. This hypothesis can be confirmed by the additional results that the selective antagonist targeting PPARγ but not α and β effectively reversed PFNA exposure–related smaller follicle size, less ovarian steroidogenesis, disrupted ovulation, and lower expression FSH/LH target genes. Moreover, the rescuing effects of PPARγ antagonist (GW9662) on PFNA exposure–related ovulation failure in eIVFG model were validated *in vivo* using mouse superovulation model. Together, these results suggest that in mice, PFNA can act as a selective PPARγ agonist in granulosa cells to interfere with gonadotropin-dependent follicle growth, steroidogenesis, and ovulation.

The phase-out of legacy long-chain PFAS makes short-chain PFAS increasingly manufactured and applied as alternatives.[2,3] There are currently no regulatory guidelines regarding the use and safety levels of short-chain PFAS, and their impacts or toxic mechanism on female reproductive health remain inadequately studied. In comparison with long-chain PFAS, short-chain PFAS may have faster elimination rates and shorter half-lives.[22,68] A recent study reported that short-chain PFAS had weaker binding affinity toward PPARs, which may result in less toxicity in the Atlantic cod.[69] Another *in vivo* study conducted by the US National Toxicology Program (NTP) showed that in young adult female rats orally exposed to long-chain PFOS (C8) or short-chain PFBS (C4) for 28 d, PFBS required a much higher dose (250–1,000 mg/kg) to disrupt rat estrous cyclicities to an extent similar to PFOS (5 mg/kg).[156] Our results are in line with these findings and revealed that all three short-chain PFAS did not affect follicle reproductive outcomes as the long-chain PFAS did. However, we are cautious to make any conclusions about the safety of short-chain vs. long-chain PFAS on female reproduction for several reasons. First, in comparison with long-chain PFAS, short-chain PFAS have a lower adsorption potential, making them highly mobile,[157,158] more prone to reach and contaminate

water sources, and more difficult to be removed by large scale filtration systems.[159–161] Second, short-chain PFAS might be as persistent as long-chain PFAS,[162] leading to an increase in their environmental distribution and accumulation due to the growing use of short-chain PFAS as substitutes. Third, although short-chain PFAS have shorter half-lives,[163] their environmental persistence and high contamination levels may result in continuous and chronic exposures in humans,[164] raising concerns about the harmful health impacts of the long-term exposure.[165] Fourth, short-chain PFAS have been found to have a high affinity for binding to serum albumin,[166,167] which could lead to a high distribution and concentration in highly vascularized tissues, including antral follicles. Last but not least, short-chain PFAS have been shown to exhibit similar or even more toxic effects than long-chain PFAS in nonreproductive tissues through similar or distinct toxic mechanisms in a placental trophoblast model,[79] human cell lines,[168] and liver organoids.[169] Although we did not identify any significant morphological or hormonal differences in follicles treated with short-chain PFAS in comparison with controls, we cannot rule out the possibility that short-chain PFAS, such as GenX, did not perturb follicular health at molecular levels. These facts highlight the need for in-depth studies to fully understand their female reproductive impact.

Despite our findings (less follicle growth, lower hormone secretion, and less ovulation) from the Tier 1 *in vitro* analysis suggested that the long-chain but not short-chain PFAS exhibited ovarian-disrupting effects, those long-chain PFAS had distinct effects on different follicular end points. The chemical structure of PFAS, especially the length of carbon backbone chains and functional groups attached, has been shown to contribute to the toxicity of different PFAS congeners.[170] Here, we advanced PFNA for mechanistic assessments and *in vivo* verification but did not perform similar studies for PFOA/S and short-chain PFAS. Moreover, previous studies reported discrepancies in PPARs between mice and humans, such as the lower sensitivities in humans to PPARα activators due to a lower PPARα expression
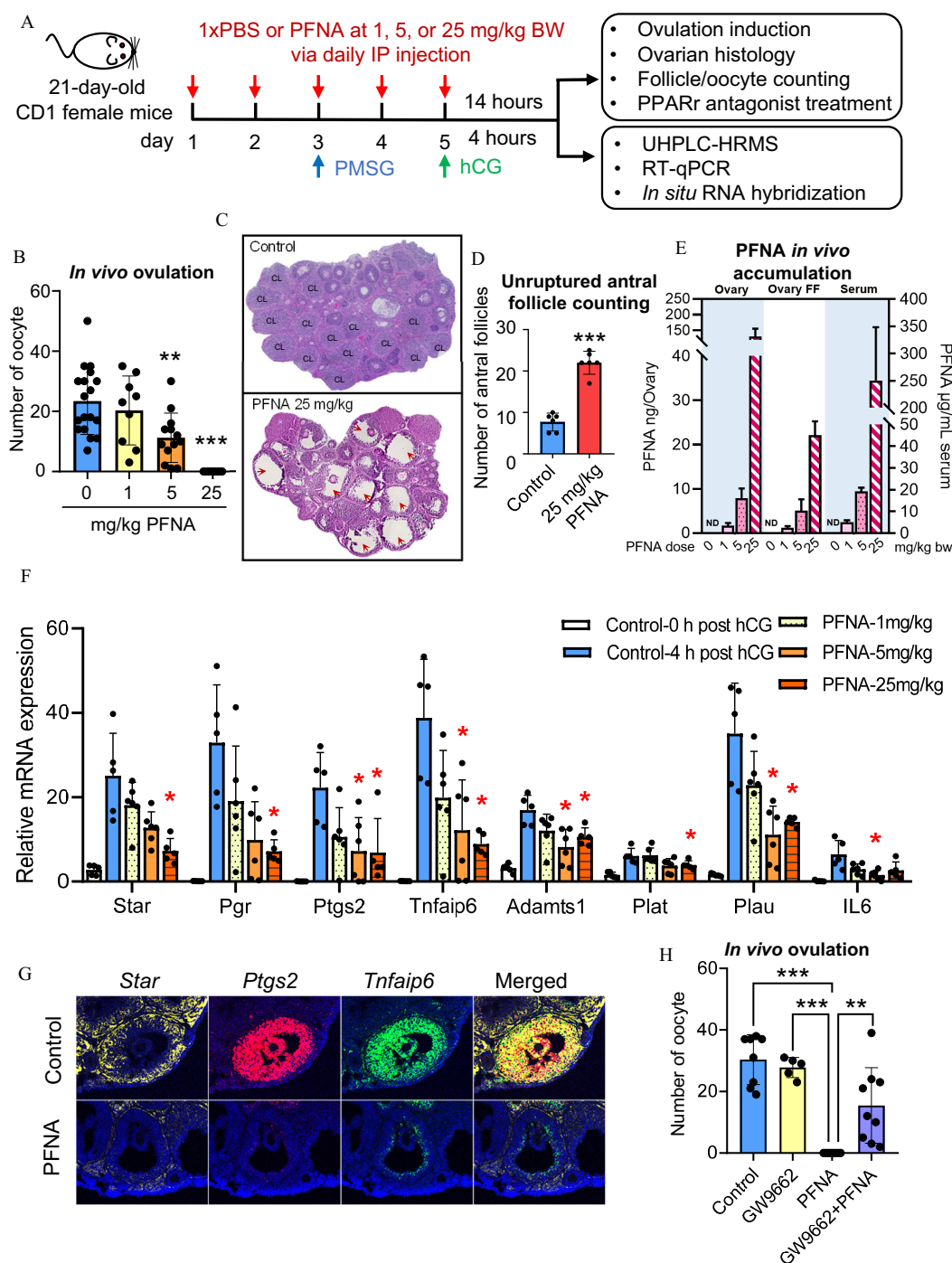
**Figure 10.** Effects of PFNA on ovulation in a mouse superovulation model. (A) Schematic of the superovulation model and PFNA exposure *in vivo*. (B) Average numbers of ovulated oocytes collected from prepubertal mice treated with vehicle ($n=18$), 1 ($n=9$), 5 ($n=13$), and 25 ($n=9$) mg/kg of PFNA; asterisk indicates the significant difference from different PFNA dose groups to the control group (0 mg/kg PFNA). (C) Representative images of ovary histology from mice treated with PBS and 25 mg/kg PFNA. Red arrows indicate unovulated late-stage antral follicles. (D) Average number of antral follicles in mice treated with PBS ($n=5$) or 25 mg/kg PFNA ($n=5$). (E) Analytical measurement of PFNA in the serum, whole ovary, or FF of large antral follicles ($n=3–4$). The amount of PFNA in the whole ovary and ovary FF is referred to the left *y*-axis (PFNA ng per ovary). The concentration of PFNA in serum is referred to the right *y*-axis (PFNA µg/mL serum). (F) Relative mRNA expression of ovulation-related genes at 4 h post hCG injection examined by RT-qPCR ($n=5$ in the control and $n=5$ in the PFNA treatment group). Expression data were normalized with *Gapdh*. Asterisk indicates the significant difference from different PFNA dose groups to the control 4 h post-hCG group (0 µM). (G) Representative images of *in situ* hybridization of large antral follicles treated with vehicle or PFNA at 4 h post hCG injection. (H) Average numbers of ovulated oocytes collected from mice treated with PBS ($n=8$), 1 mg/kg PPARγ antagonist (GW9662) ($n=5$), 25 mg/kg PFNA ($n=8$), or cotreatment of PPARγ antagonist (GW9662) and PFNA ($n=9$); asterisk indicates the significant difference between two connected groups. Data were analyzed with Student's *t*-test (B,D). Error bars: mean ± SD. Data in Figure 10 are presented in Excel Table S19. Note: FF, follicular fluid; *Gapdh*, glyceraldehyde-3-phosphate dehydrogenase; hCG, human chorionic gonadotrophin; ND, nondetectable; PBS, phosphate-buffered saline; PFNA, perfluorononanoic acid; PPARγ, peroxisome proliferator–activated receptor gamma; RT-qPCR, reverse transcription–quantitative polymerase chain reaction; SD, standard deviation. $^*p < 0.05$; $^{**}p < 0.01$.
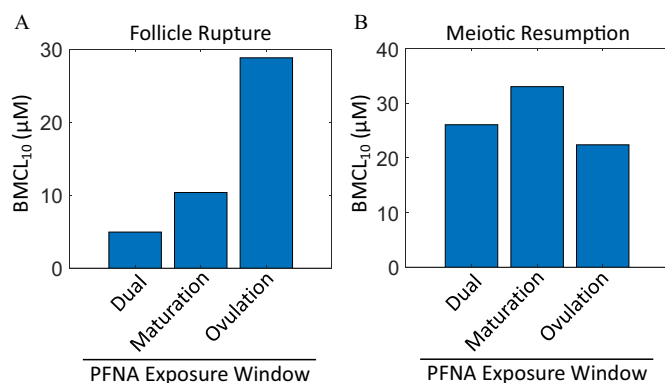
**Figure 11.** BMCL$_{10}$ of PFNA for dual-, maturation-, and ovulation-window exposures as indicated for *in vitro* follicle rupture (A) and meiotic resumption (B). Data presented in this figure are also included in Excel Table S5–S7. Note: BMCL, benchmark concentration lower confidence limit; BMD, benchmark dose modeling; PFNA, perfluorononanoic acid.

and DNA binding affinity in comparison with rodents, and different metabolic features such as the glucose–insulin singling pathway between mouse and human PPARγ mutants.[171–173] In addition, diet conditions may also affect the toxicity of PFAS. For example, the high-fat and low fiber diets have been associated with higher PFAS accumulation,[174] and diets rich in antioxidants (e.g., vitamins C and E) may mitigate PFAS-induced oxidative stress.[175] Collectively, advanced investigations regarding the roles of different PPAR isoforms, structurally different PFAS congeners, diets, and species differences in PFAS-induced ovarian toxicity are needed in future studies.

In line with folliculogenesis, the follicle-enclosed oocyte produces and accumulates maternal factors, such as mRNAs, proteins, and organelles, to acquire both meiotic and developmental competence to enable subsequent fertilization and early embryogenesis.[176] Successful oogenesis relies on the bidirectional communication between oocytes and surrounding somatic cells.[177,178] *In vitro* exposure of denuded oocytes to PFNA has been shown to affect oocyte maturation by inducing oxidative stress,[66] indicating that PFAS may directly affect oocytes. Our results showed that there was a significant reduction in the percentage of ovulated MII oocytes released from PFAS-treated follicles. However, it is unclear whether this oocyte meiotic disorder is a direct perturbation of PFAS on oocytes, an indirect effect through granulosa cells, or both. In addition to somatic granulosa cells, PPARγ has also been detected in mammalian oocytes.[143,179] Thus, future studies should determine whether PFAS can accumulate in oocytes and compromise oocyte quality by interfering with oogenic PPARγ and related signaling.

The results obtained from both an *in vitro* ovarian follicle culture system and an *in vivo* mouse model here suggested the ovarian-disrupting effects of long-chain PFAS and the mechanisms via PPARγ. It is important to acknowledge several limitations that needed to be addressed in our future studies. First, the follicle culture system used a constant FSH concentration, which does not recapitulate the dynamic secretion of gonadotropins and lacks the negative and positive feedback control of the hypothalamus–pituitary–gonad (HPG) axis. Second, the regulatory signals and gene expression patterns involved in follicle development and ovulation are complex. Thus, the ratio of up-/down-regulated DEGs may not entirely reflect the activation/deactivation status of the corresponding enriched process or pathway in the PFNA-treated follicles, warranting further investigation in the future. Third, we primarily focused on PFNA for mechanistic studies because PFNA

is a relatively lesser-studied long-chain PFAS in comparison with the legacy PFOA/S, and it also showed ovarian-disrupting effects (e.g., altered hormone secretion and failed ovulation). An in-depth mechanistic investigation of all other short-chain and long-chain PFAS is further needed to narrow down pathways implicated in the failure of certain ovarian functions and identify potential PFAS related biomarkers. Fourth, more comprehensive ovarian morphometry and investigations into the underlying mechanisms of the ovarian impacts of PFNA are essential in future studies. As evidenced by the remarkable difference of ovarian histology between the control and PFNA treatment groups, there might be more toxic effects caused by PFNA, such as the ovary volume, ovarian stroma, and percentages of different stages of follicles. Last, we primarily focused on the ovarian impacts of a single PFAS, but humans are exposed to PFAS in mixtures. Moreover, the mouse superovulation model and PFAS exposure via IP injection do not fully recapitulate the real-world exposure scenario of PFAS in humans. Therefore, long-term oral exposure (e.g., via drinking water) to PFAS and mixtures in a naturally cycling mouse model needs to be considered in future studies.

In conclusion, we demonstrate the ovarian-disrupting effects of PFAS in a mouse *in vitro* and *in vivo* model. Our results suggested that PFNA, a long-chain PFAS that can have similar environmental contamination levels to the legacy PFOA/S, accumulated in the ovary and acted as a PPARγ agonist in follicular granulosa cells to interfere with follicle growth, ovulation, and hormone secretion. There is an urgent need to reduce or eliminate exposure to PFAS to safeguard women's reproductive health and fertility.

## Acknowledgments

## References

1. Buck RC, Franklin J, Berger U, Conder JM, Cousins IT, de Voogt P, et al. 2011. Perfluoroalkyl and polyfluoroalkyl substances in the environment: terminology, classification, and origins. Integr Environ Assess Manag 7(4):513–541, PMID: 21793199, https://doi.org/10.1002/ieam.258.
2. Heydebreck F, Tang J, Xie Z, Ebinghaus R. 2015. Alternative and legacy perfluoroalkyl substances: differences between European and Chinese river/estuary systems. Environ Sci Technol 49(14):8386–8395, PMID: 26106903, https://doi.org/10.1021/acs.est.5b01648.
3. Gebbink WA, van Asseldonk L, van Leeuwen SPJ. 2017. Presence of emerging per- and polyfluoroalkyl substances (PFASs) in river and

drinking water near a fluorochemical production plant in the Netherlands. Environ Sci Technol 51(19):11057–11065, PMID: 28853567, https://doi.org/10.1021/acs.est.7b02488.

4. Gangal SV. 2004. Perfluorinated polymers. In: *Kirk-Othmer Encyclopedia of Chemical Technology.* Hoboken, NJ: John Wiley & Sons, Inc., 1–68.

5. Lindstrom AB, Strynar MJ, Libelo EL. 2011. Polyfluorinated compounds: past, present, and future. Environ Sci Technol 45(19):7954–7961, PMID: 21866930, https://doi.org/10.1021/es2011622.

6. US FDA (US Food and Drug Administration). *Per and Polyfluoroalkyl Substances (PFAS).* Washington, DC: US FDA.

7. Place BJ, Field JA. 2012. Identification of novel fluorochemicals in aqueous film-forming foams used by the US military. Environ Sci Technol 46(13):7120–7127, PMID: 22681548, https://doi.org/10.1021/es301465n.

8. Mariussen E. 2012. Neurotoxic effects of perfluoroalkylated compounds: mechanisms of action and environmental relevance. Arch Toxicol 86(9):1349–1367, PMID: 22456834, https://doi.org/10.1007/s00204-012-0822-6.

9. Conder JM, Hoke RA, De Wolf W, Russell MH, Buck RC. 2008. Are PFCAs bioaccumulative? A critical review and comparison with regulatory criteria and persistent lipophilic compounds. Environ Sci Technol 42(4):995–1003, PMID: 18351063, https://doi.org/10.1021/es070895g.

10. US Congress House Committee on Oversight and Accountability. 2019. Toxic, Forever Chemicals: A Call for Immediate Federal Action on PFAS. https://oversightdemocrats.house.gov/legislation/hearings/toxic-forever-chemicals-a-call-for-immediate-federal-action-on-pfas [accessed 20 August 2022].

11. Paul AG, Jones KC, Sweetman AJ. 2009. A first global production, emission, and environmental inventory for perfluorooctane sulfonate. Environ Sci Technol 43(2):386–392, PMID: 19238969, https://doi.org/10.1021/es802216n.

12. Trudel D, Horowitz L, Wormuth M, Scheringer M, Cousins IT, Hungerbuhler K. 2008. Estimating consumer exposure to PFOS and PFOA. Risk Anal 28(2):251–269, PMID: 18419647, https://doi.org/10.1111/j.1539-6924.2008.01017.x.

13. Daly ER, Chan BP, Talbot EA, Nassif J, Bean C, Cavallo SJ, et al. 2018. Per- and polyfluoroalkyl substance (PFAS) exposure assessment in a community exposed to contaminated drinking water, New Hampshire, 2015. Int J Hyg Environ Health 221(3):569–577, PMID: 29514764, https://doi.org/10.1016/j.ijheh.2018.02.007.

14. Hu XC, Andrews DQ, Lindstrom AB, Bruton TA, Schaider LA, Grandjean P, et al. 2016. Detection of poly- and perfluoroalkyl substances (PFASs) in U.S. drinking water linked to industrial sites, military fire training areas, and wastewater treatment plants. Environ Sci Technol Lett 3(10):344–350, PMID: 27752509, https://doi.org/10.1021/acs.estlett.6b00260.

15. Guelfo JL, Adamson DT. 2018. Evaluation of a national data set for insights into sources, composition, and concentrations of per- and polyfluoroalkyl substances (PFASs) in U.S. drinking water. Environ Pollut 236:505–513, PMID: 29427949, https://doi.org/10.1016/j.envpol.2018.01.066.

16. Sunderland EM, Hu XC, Dassuncao C, Tokranov AK, Wagner CC, Allen JG. 2019. A review of the pathways of human exposure to poly- and perfluoroalkyl substances (PFASs) and present understanding of health effects. J Expo Sci Environ Epidemiol 29(2):131–147, PMID: 30470793, https://doi.org/10.1038/s41370-018-0094-1.

17. EWG (Environmental Working Group). 2018. Report: Up to 110 Million Americans Could Have PFAS-Contaminated Drinking Water. https://www.ewg.org/research/report-110-million-americans-could-have-pfas-contaminated-drinking-water#:~:text=Based%20on%20this%20data%2C%20EWG's,EWG's%20national%20Tap%20Water%20Database [accessed 20 August 2022].

18. Goldenman G, Fernandes M, Holland M, Tugran T, Nordin A, Schoumacher C, et al. 2019. *The Cost of Inaction: A Socioeconomic Analysis of Environmental and Health Impacts Linked to Exposure To PFAS.* Copenhagen, Denmark: Nordic Council of Ministers.

19. Banwell C, Housen T, Smurthwaite K, Trevenar S, Walker L, Todd K, et al. 2021. Health and social concerns about living in three communities affected by per- and polyfluoroalkyl substances (PFAS): a qualitative study in Australia. PLoS One 16(1):e0245141, PMID: 33444329, https://doi.org/10.1371/journal.pone.0245141.

20. Olsen GW, Burris JM, Ehresman DJ, Froehlich JW, Seacat AM, Butenhoff JL, et al. 2007. Half-life of serum elimination of perfluorooctanesulfonate, perfluorohexanesulfonate, and perfluorooctanoate in retired fluorochemical production workers. Environ Health Perspect 115(9):1298–1305, PMID: 17805419, https://doi.org/10.1289/ehp.10009.

21. Kemper RA, Nabb DL. 2005. In vitro studies in microsomes from rat and human liver, kidney, and intestine suggest that perfluorooctanoic acid is not a substrate for microsomal UDP-glucuronosyltransferases. Drug Chem Toxicol 28(3):281–287, PMID: 16051554, https://doi.org/10.1081/dct-200064468.

22. Xu Y, Fletcher T, Pineda D, Lindh CH, Nilsson C, Glynn A, et al. 2020. Serum half-lives for short- and long-chain perfluoroalkyl acids after ceasing exposure from drinking water contaminated by firefighting foam. Environ Health Perspect 128(7):077004, PMID: 32648786, https://doi.org/10.1289/EHP6785.

23. Kato K, Wong LY, Jia LT, Kuklenyik Z, Calafat AM. 2011. Trends in exposure to polyfluoroalkyl chemicals in the U.S. population: 1999–2008. Environ Sci Technol 45(19):8037–8045, PMID: 21469664, https://doi.org/10.1021/es1043613.

24. Toms L-ML, Thompson J, Rotander A, Hobson P, Calafat AM, Kato K, et al. 2014. Decline in perfluorooctane sulfonate and perfluorooctanoate serum concentrations in an Australian population from 2002 to 2011. Environ Int 71:74–80, PMID: 24980755, https://doi.org/10.1016/j.envint.2014.05.019.

25. Pitter G, Da Re F, Canova C, Barbieri G, Zare Jeddi M, Daprà F, et al. 2020. Serum levels of perfluoroalkyl substances (PFAS) in adolescents and young adults exposed to contaminated drinking water in the Veneto Region, Italy: a cross-sectional study based on a health surveillance program. Environ Health Perspect 128(2):027007, PMID: 32068468, https://doi.org/10.1289/EHP5337.

26. Lee JH, Lee CK, Suh CH, Kang HS, Hong CP, Choi SN. 2017. Serum concentrations of per- and poly-fluoroalkyl substances and factors associated with exposure in the general adult population in South Korea. Int J Hyg Environ Health 220(6):1046–1054, PMID: 28688604, https://doi.org/10.1016/j.ijheh.2017.06.005.

27. Wang W, Zhou W, Wu S, Liang F, Li Y, Zhang J, et al. 2019. Perfluoroalkyl substances exposure and risk of polycystic ovarian syndrome related infertility in Chinese women. Environ Pollut 247:824–831, PMID: 30731307, https://doi.org/10.1016/j.envpol.2019.01.039.

28. Heffernan AL, Cunningham TK, Drage DS, Aylward LL, Thompson K, Vijayasarathy S, et al. 2018. Perfluorinated alkyl acids in the serum and follicular fluid of UK women with and without polycystic ovarian syndrome undergoing fertility treatment and associations with hormonal and metabolic parameters. Int J Hyg Environ Health 221(7):1068–1075, PMID: 30037723, https://doi.org/10.1016/j.ijheh.2018.07.009.

29. Graber JM, Alexander C, Laumbach RJ, Black K, Strickland PO, Georgopoulos PG, et al. 2019. Per and polyfluoroalkyl substances (PFAS) blood levels after contamination of a community water supply and comparison with 2013–2014 NHANES. J Expo Sci Environ Epidemiol 29(2):172–182, PMID: 30482936, https://doi.org/10.1038/s41370-018-0096-z.

30. Shen J, Mao Y, Zhang H, Lou H, Zhang L, Moreira JP, et al. 2024. Exposure of women undergoing *in-vitro* fertilization to per-and polyfluoroalkyl substances: evidence on negative effects on fertilization and high-quality embryos. Environ Pollut 359:124474, PMID: 38992828, https://doi.org/10.1016/j.envpol.2024.124474.

31. Kang Q, Gao F, Zhang X, Wang L, Liu J, Fu M, et al. 2020. Nontargeted identification of per- and polyfluoroalkyl substances in human follicular fluid and their blood-follicle transfer. Environ Int 139:105686, PMID: 32278886, https://doi.org/10.1016/j.envint.2020.105686.

32. Olsen GW, Burris JM, Mandel JH, Zobel LR. 1999. Serum perfluorooctane sulfonate and hepatic and lipid clinical chemistry tests in fluorochemical production employees. J Occup Environ Med 41(9):799–806, PMID: 10491796, https://doi.org/10.1097/00043764-199909000-00012.

33. Olsen GW, Zobel LR. 2007. Assessment of lipid, hepatic, and thyroid parameters with serum perfluorooctanoate (PFOA) concentrations in fluorochemical production workers. Int Arch Occup Environ Health 81(2):231–246, PMID: 17605032, https://doi.org/10.1007/s00420-007-0213-0.

34. Olsen GW, Burris JM, Burlew MM, Mandel JH. 2003. Epidemiologic assessment of worker serum perfluorooctanesulfonate (PFOS) and perfluorooctanoate (PFOA) concentrations and medical surveillance examinations. J Occup Environ Med 45(3):260–270, PMID: 12661183, https://doi.org/10.1097/01.jom.0000052958.59271.10.

35. Innes KE, Ducatman AM, Luster MI, Shankar A. 2011. Association of osteoarthritis with serum levels of the environmental contaminants perfluorooctanoate and perfluorooctane sulfonate in a large Appalachian population. Am J Epidemiol 174(4):440–450, PMID: 21709135, https://doi.org/10.1093/aje/kwr107.

36. Bartell SM, Calafat AM, Lyu C, Kato K, Ryan PB, Steenland K. 2010. Rate of decline in serum PFOA concentrations after granular activated carbon filtration at two public water systems in Ohio and West Virginia. Environ Health Perspect 118(2):222–228, PMID: 20123620, https://doi.org/10.1289/ehp.0901252.

37. Benninghoff AD, Orner GA, Buchner CH, Hendricks JD, Duffy AM, Williams DE. 2012. Promotion of hepatocarcinogenesis by perfluoroalkyl acids in rainbow trout. Toxicol Sci 125(1):69–78, PMID: 21984479, https://doi.org/10.1093/toxsci/kfr267.

38. Das KP, Wood CR, Lin MT, Starkov AA, Lau C, Wallace KB, et al. 2017. Perfluoroalkyl acids-induced liver steatosis: effects on genes controlling lipid homeostasis. Toxicology 378:37–52, PMID: 28049043, https://doi.org/10.1016/j.tox.2016.12.007.

39. Shearer JJ, Callahan CL, Calafat AM, Huang W-Y, Jones RR, Sabbisetti VS, et al. 2021. Serum concentrations of per- and polyfluoroalkyl substances and risk of renal cell carcinoma. J Natl Cancer Inst 113(5):580–587, PMID: 32944748, https://doi.org/10.1093/jnci/djaa143.

40. Peden-Adams MM, EuDaly JG, Dabra S, EuDaly A, Heesemann L, Smythe J, et al. 2007. Suppression of humoral immunity following exposure to the perfluorinated insecticide sulfluramid. J Toxicol Environ Health A 70(13):1130–1141, PMID: 17558808, https://doi.org/10.1080/15287390701252733.

41. Yang Q, Abedi-Valugerdi M, Xie Y, Zhao X-Y, Möller G, Nelson BD, et al. 2002. Potent suppression of the adaptive immune response in mice upon dietary

exposure to the potent peroxisome proliferator, perfluorooctanoic acid. Int Immunopharmacol 2(2–3):389–397, PMID: 11811941, https://doi.org/10.1016/s1567-5769(01)00164-3.

42. Rosen EM, Kotlarz N, Knappe DRU, Lea CS, Collier DN, Richardson DB, et al. 2022. Drinking water-associated PFAS and fluoroethers and lipid outcomes in the GenX exposure study. Environ Health Perspect 130(9):097002, PMID: 36069575, https://doi.org/10.1289/EHP11033.

43. Jørgensen KT, Specht IO, Lenters V, Bach CC, Rylander L, Jönsson BA, et al. 2014. Perfluoroalkyl substances and time to pregnancy in couples from Greenland, Poland and Ukraine. Environ Health 13:116, PMID: 25533644, https://doi.org/10.1186/1476-069X-13-116.

44. Steenland K, Barry V, Savitz D. 2018. Serum perfluorooctanoic acid and birthweight: an updated meta-analysis with bias analysis. Epidemiology 29(6):765–776, PMID: 30063543, https://doi.org/10.1097/EDE.0000000000000903.

45. Zhang S, Tan R, Pan R, Xiong J, Tian Y, Wu J, et al. 2018. Association of perfluoroalkyl and polyfluoroalkyl substances with premature ovarian insufficiency in Chinese women. J Clin Endocrinol Metab 103(7):2543–2551, PMID: 29986037, https://doi.org/10.1210/jc.2017-02783.

46. Taylor KW, Hoffman K, Thayer KA, Daniels JL. 2014. Polyfluoroalkyl chemicals and menopause among women 20-65 years of age (NHANES). Environ Health Perspect 122(2):145–150, PMID: 24280566, https://doi.org/10.1289/ehp.1306707.

47. Di Nisio A, Rocca MS, Sabovic I, De Rocco Ponce M, Corsini C, Guidolin D, et al. 2020. Perfluorooctanoic acid alters progesterone activity in human endometrial cells and induces reproductive alterations in young women. Chemosphere 242:125208, PMID: 31896193, https://doi.org/10.1016/j.chemosphere.2019.125208.

48. Vagi SJ, Azziz-Baumgartner E, Sjödin A, Calafat AM, Dumesic D, Gonzalez L, et al. 2014. Exploring the potential association between brominated diphenyl ethers, polychlorinated biphenyls, organochlorine pesticides, perfluorinated compounds, phthalates, and bisphenol A in polycystic ovary syndrome: a case-control study. BMC Endocr Disord 14:86, PMID: 25348326, https://doi.org/10.1186/1472-6823-14-86.

49. Velez MP, Arbuckle TE, Fraser WD. 2015. Maternal exposure to perfluorinated chemicals and reduced fecundity: the MIREC study. Hum Reprod 30(3):701–709, PMID: 25567616, https://doi.org/10.1093/humrep/deu350.

50. Fei C, McLaughlin JK, Lipworth L, Olsen J. 2009. Maternal levels of perfluorinated chemicals and subfecundity. Hum Reprod 24(5):1200–1205, PMID: 19176540, https://doi.org/10.1093/humrep/den490.

51. La Rocca C, Alessi E, Bergamasco B, Caserta D, Ciardo F, Fanello E, et al. 2012. Exposure and effective dose biomarkers for perfluorooctane sulfonic acid (PFOS) and perfluorooctanoic acid (PFOA) in infertile subjects: preliminary results of the PREVIENI project. Int J Hyg Environ Health 215(2):206–211, PMID: 22197512, https://doi.org/10.1016/j.ijheh.2011.10.016.

52. Kumar TR, Wang Y, Lu N, Matzuk MM. 1997. Follicle stimulating hormone is required for ovarian follicle maturation but not male fertility. Nat Genet 15(2):201–204, PMID: 9020850, https://doi.org/10.1038/ng0297-201.

53. Dierich A, Sairam MR, Monaco L, Fimia GM, Gansmuller A, LeMeur M, et al. 1998. Impairing follicle-stimulating hormone (FSH) signaling in vivo: targeted disruption of the FSH receptor leads to aberrant gametogenesis and hormonal imbalance. Proc Natl Acad Sci USA 95(23):13612–13617, PMID: 9811848, https://doi.org/10.1073/pnas.95.23.13612.

54. Zhang FP, Poutanen M, Wilbertz J, Huhtaniemi I. 2001. Normal prenatal but arrested postnatal sexual development of luteinizing hormone receptor knockout (LuRKO) mice. Mol Endocrinol 15(1):172–183, PMID: 11145748, https://doi.org/10.1210/mend.15.1.0582.

55. Pakarainen T, Zhang FP, Nurmi L, Poutanen M, Huhtaniemi I. 2005. Knockout of luteinizing hormone receptor abolishes the effects of follicle-stimulating hormone on preovulatory maturation and ovulation of mouse graafian follicles. Mol Endocrinol 19(10):2591–2602, PMID: 15941853, https://doi.org/10.1210/me.2005-0075.

56. Austin ME, Kasturi BS, Barber M, Kannan K, MohanKumar PS, MohanKumar SM. 2003. Neuroendocrine effects of perfluorooctane sulfonate in rats. Environ Health Perspect 111(12):1485–1489, PMID: 12948888, https://doi.org/10.1289/ehp.6128.

57. Feng X, Wang X, Cao X, Xia Y, Zhou R, Chen L. 2015. Chronic exposure of female mice to an environmental level of perfluorooctane sulfonate suppresses estrogen synthesis through reduced histone H3K14 acetylation of the StAR promoter leading to deficits in follicular development and ovulation. Toxicol Sci 148(2):368–379, PMID: 26358002, https://doi.org/10.1093/toxsci/kfv197.

58. Zhang Y, Cao X, Chen L, Qin Y, Xu Y, Tian Y, et al. 2020. Exposure of female mice to perfluorooctanoic acid suppresses hypothalamic kisspeptin-reproductive endocrine system through enhanced hepatic fibroblast growth factor 21 synthesis, leading to ovulation failure and prolonged dioestrus. J Neuroendocrinol 32(5):e12848, PMID: 32307816, https://doi.org/10.1111/jne.12848.

59. Yang M, Lee Y, Gao L, Chiu K, Meling DD, Flaws JA, et al. 2022. Perfluorooctanoic acid disrupts ovarian steroidogenesis and folliculogenesis in adult mice. Toxicol Sci 186(2):260–268, PMID: 35104888, https://doi.org/10.1093/toxsci/kfac005.

60. Miller WL, Auchus RJ. 2011. The molecular biology, biochemistry, and physiology of human steroidogenesis and its disorders. Endocr Rev 32(1):81–151, PMID: 21051590, https://doi.org/10.1210/er.2010-0013.

61. Chaparro-Ortega A, Betancourt M, Rosas P, Vázquez-Cuevas FG, Chavira R, Bonilla E, et al. 2018. Endocrine disruptor effect of perfluorooctane sulfonic acid (PFOS) and perfluorooctanoic acid (PFOA) on porcine ovarian cell steroidogenesis. Toxicol In Vitro 46:86–93, PMID: 28982594, https://doi.org/10.1016/j.tiv.2017.09.030.

62. Seacat AM, Thomford PJ, Hansen KJ, Olsen GW, Case MT, Butenhoff JL. 2002. Subchronic toxicity studies on perfluorooctanesulfonate potassium salt in cynomolgus monkeys. Toxicol Sci 68(1):249–264, PMID: 12075127, https://doi.org/10.1093/toxsci/68.1.249.

63. Domínguez A, Salazar Z, Arenas E, Betancourt M, Ducolomb Y, González-Márquez H, et al. 2016. Effect of perfluorooctane sulfonate on viability, maturation and gap junctional intercellular communication of porcine oocytes in vitro. Toxicol In Vitro 35:93–99, PMID: 27233358, https://doi.org/10.1016/j.tiv.2016.05.011.

64. López-Arellano P, López-Arellano K, Luna J, Flores D, Jiménez-Salazar J, Gavia G, et al. 2019. Perfluorooctanoic acid disrupts gap junction intercellular communication and induces reactive oxygen species formation and apoptosis in mouse ovaries. Environ Toxicol 34(1):92–98, PMID: 30277307, https://doi.org/10.1002/tox.22661.

65. Hallberg I, Kjellgren J, Persson S, Orn S, Sjunnesson Y. 2019. Perfluorononanoic acid (PFNA) alters lipid accumulation in bovine blastocysts after oocyte exposure during in vitro maturation. Reprod Toxicol 84:1–8, PMID: 30502403, https://doi.org/10.1016/j.reprotox.2018.11.005.

66. Jiao X, Liu N, Xu Y, Qiao H. 2021. Perfluorononanoic acid impedes mouse oocyte maturation by inducing mitochondrial dysfunction and oxidative stress. Reprod Toxicol 104:58–67, PMID: 34246765, https://doi.org/10.1016/j.reprotox.2021.07.002.

67. EWG. Military Sites with Known or Suspected Discharges of PFAS. https://www.ewg.org/interactive-maps/2020-military-pfas-sites/map/ [accessed 9 January 2023].

68. Chengelis CP, Kirkpatrick JB, Myers NR, Shinohara M, Stetson PL, Sved DW. 2009. Comparison of the toxicokinetic behavior of perfluorohexanoic acid (PFHxA) and nonafluorobutane-1-sulfonic acid (PFBS) in cynomolgus monkeys and rats. Reprod Toxicol 27(3–4):400–406, PMID: 19429410, https://doi.org/10.1016/j.reprotox.2009.01.013.

69. Søderstrøm S, Lille-Langøy R, Yadetie F, Rauch M, Milinski A, Dejaegere A, et al. 2022. Agonistic and potentiating effects of perfluoroalkyl substances (PFAS) on the Atlantic cod (Gadus morhua) peroxisome proliferator-activated receptors (Ppars). Environ Int 163:107203, PMID: 35364415, https://doi.org/10.1016/j.envint.2022.107203.

70. Zhang L, Ren XM, Wan B, Guo LH. 2014. Structure-dependent binding and activation of perfluorinated compounds on human peroxisome proliferator-activated receptor gamma. Toxicol Appl Pharmacol 279(3):275–283, PMID: 24998974, https://doi.org/10.1016/j.taap.2014.06.020.

71. Froment P, Fabre S, Dupont J, Pisselet C, Chesneau D, Staels B, et al. 2003. Expression and functional role of peroxisome proliferator-activated receptor-gamma in ovarian folliculogenesis in the sheep. Biol Reprod 69(5):1665–1674, PMID: 12890736, https://doi.org/10.1095/biolreprod.103.017244.

72. Komar CM, Braissant O, Wahli W, Curry TE Jr. 2001. Expression and localization of PPARs in the rat ovary during follicular development and the periovulatory period. Endocrinology 142(11):4831–4838, PMID: 11606451, https://doi.org/10.1210/endo.142.11.8429.

73. Banerjee J, Komar CM. 2006. Effects of luteinizing hormone on peroxisome proliferator-activated receptor gamma in the rat ovary before and after the gonadotropin surge. Reproduction 131(1):93–101, PMID: 16388013, https://doi.org/10.1530/rep.1.00730.

74. Ferst JG, Rovani MT, Dau AMP, Gasperin BG, Antoniazzi AQ, Bordignon V, et al. 2020. Activation of PPARG inhibits dominant follicle development in cattle. Theriogenology 142:276–283, PMID: 31708195, https://doi.org/10.1016/j.theriogenology.2019.10.032.

75. Jiang C, Ting AT, Seed B. 1998. PPAR-gamma agonists inhibit production of monocyte inflammatory cytokines. Nature 391(6662):82–86, PMID: 9422509, https://doi.org/10.1038/34184.

76. Yu JH, Kim KH, Kim H. 2008. SOCS 3 and PPAR-gamma ligands inhibit the expression of IL-6 and TGF-beta1 by regulating JAK2/STAT3 signaling in pancreas. Int J Biochem Cell Biol 40(4):677–688, PMID: 18035585, https://doi.org/10.1016/j.biocel.2007.10.007.

77. National Research Council Committee for the Update of the Guide for the Care and Use of Laboratory Animals. 2011. Guide for the Care and Use of Laboratory Animals. 8th ed. Washington, DC: National Academies Press.

78. Liberatore HK, Jackson SR, Strynar MJ, McCord JP. 2020. Solvent suitability for HFPO-DA ("GenX" parent acid) in toxicological studies. Environ Sci Technol Lett 7(7):477–481, PMID: 32944590, https://doi.org/10.1021/acs.estlett.0c00323.

79. Bangma J, Szilagyi J, Blake BE, Plazas C, Kepper S, Fenton SE, et al. 2020. An assessment of serum-dependent impacts on intracellular accumulation and genomic response of per- and polyfluoroalkyl substances in a placental trophoblast model. Environ Toxicol 35(12):1395–1405, PMID: 32790152, https://doi.org/10.1002/tox.23004.

80. Smeltz MG, Clifton MS, Henderson WM, McMillan L, Wetmore BA. 2023. Targeted per- and polyfluoroalkyl substances (PFAS) assessments for high throughput screening: analytical and testing considerations to inform a PFAS stock quality evaluation framework. Toxicol Appl Pharmacol 459:116355, PMID: 36535553, https://doi.org/10.1016/j.taap.2022.116355.

81. Modrzyński JJ, Christensen JH, Brandt KK. 2019. Evaluation of dimethyl sulfoxide (DMSO) as a co-solvent for toxicity testing of hydrophobic organic compounds. Ecotoxicology 28(9):1136–1141, PMID: 31559559, https://doi.org/10.1007/s10646-019-02107-0.

82. Hoyberghs J, Bars C, Ayuso M, Van Ginneken C, Foubert K, Van Cruchten S. 2021. DMSO concentrations up to 1% are safe to be used in the zebrafish embryo developmental toxicity assay. Front Toxicol 3:804033, PMID: 35295145, https://doi.org/10.3389/ftox.2021.804033.

83. Kim YR, White N, Bräunig J, Vijayasarathy S, Mueller JF, Knox CL, et al. 2020. Per- and poly-fluoroalkyl substances (PFASs) in follicular fluid from women experiencing infertility in Australia. Environ Res 190:109963, PMID: 32745751, https://doi.org/10.1016/j.envres.2020.109963.

84. Xiao S, Duncan FE, Bai L, Nguyen CT, Shea LD, Woodruff TK. 2015. Size-specific follicle selection improves mouse oocyte reproductive outcomes. Reproduction 150(3):183–192, PMID: 26116002, https://doi.org/10.1530/REP-15-0175.

85. Shikanov A, Xu M, Woodruff TK, Shea LD. 2011. A method for ovarian follicle encapsulation and culture in a proteolytically degradable 3 dimensional system. J Vis Exp (49):2695, PMID: 21445043, https://doi.org/10.3791/2695.

86. Chien Y, Cheng WC, Wu MR, Jiang ST, Shen CK, Chung BC. 2013. Misregulated progesterone secretion and impaired pregnancy in Cyp11a1 transgenic mice. Biol Reprod 89(4):91, PMID: 23966322, https://doi.org/10.1095/biolreprod.113.110833.

87. Konstandi M, Cheng J, Gonzalez FJ. 2013. Sex steroid hormones regulate constitutive expression of Cyp2e1 in female mouse liver. Am J Physiol Endocrinol Metab 304(10):E1118–E1128, PMID: 23548611, https://doi.org/10.1152/ajpendo.00585.2012.

88. Wang Y, Drake RS, Russo DD, Pattarawat P, Zhang Q, Zelinski MB, et al. 2021. Vitrification preserves murine ovarian follicular cell transcriptome in a 3D encapsulated in vitro follicle growth system. Biol Reprod 105(6):1378–1380, PMID: 34591115, https://doi.org/10.1093/biolre/ioab185.

89. Povey S, Lovering R, Bruford E, Wright M, Lush M, Wain H. 2001. The HUGO gene nomenclature committee (HGNC). Hum Genet 109(6):678–680, PMID: 11810281, https://doi.org/10.1007/s00439-001-0615-0.

90. Zhang J, Goods BA, Pattarawat P, Wang Y, Haining T, Zhang Q, et al. 2023. An ex vivo ovulation system enables the discovery of novel ovulatory pathways and nonhormonal contraceptive candidates. Biol Reprod 108(4):629–644, PMID: 36708230, https://doi.org/10.1093/biolre/ioad009.

91. Jiao X, Sherman BT, Huang DW, Stephens R, Baseler MW, Lane HC, et al. 2012. DAVID-WS: a stateful web service to facilitate gene/protein list analysis. Bioinformatics 28(13):1805–1806, PMID: 22543366, https://doi.org/10.1093/bioinformatics/bts251.

92. Liao Y, Wang J, Jaehnig EJ, Shi Z, Zhang B. 2019. WebGestalt 2019: gene set analysis toolkit with revamped UIs and APIs. Nucleic Acids Res 47(W1): W199–W205, PMID: 31114916, https://doi.org/10.1093/nar/gkz401.

93. Fang L, Zhang M, Li Y, Liu Y, Cui Q, Wang N. 2016. PPARgene: a database of experimentally verified and computationally predicted PPAR target genes. PPAR Res 2016:6042162, PMID: 27148361, https://doi.org/10.1155/2016/6042162.

94. Wang L-Q, Liu T, Yang S, Sun L, Zhao Z-Y, Li L-Y, et al. 2021. Perfluoroalkyl substance pollutants activate the innate immune system through the AIM2 inflammasome. Nat Commun 12(1):2915, PMID: 34006824, https://doi.org/10.1038/s41467-021-23201-0.

95. Zhang T, Wu Q, Sun HW, Zhang XZ, Yun SH, Kannan K. 2010. Perfluorinated compounds in whole blood samples from infants, children, and adults in China. Environ Sci Technol 44(11):4341–4347, PMID: 20441147, https://doi.org/10.1021/es1002132.

96. Gad SC, Spainhour CB, Shoemake C, Pallman DRS, Stricker-Krongrad A, Downing PA, et al. 2016. Tolerable levels of nonclinical vehicles and formulations used in studies by multiple routes in multiple species with notes on methods to improve utility. Int J Toxicol 35(2):95–178, PMID: 26755718, https://doi.org/10.1177/1091581815622442.

97. Al Shoyaib A, Archie SR, Karamyan VT. 2019. Intraperitoneal route of drug administration: should it be used in experimental animal studies? Pharm Res 37(1):12, PMID: 31873819, https://doi.org/10.1007/s11095-019-2745-x.

98. Lukas G, Brindle SD, Greengard P. 1971. The route of absorption of intraperitoneally administered compounds. J Pharmacol Exp Ther 178(3):562–564, PMID: 5571904.

99. Xiao S, Zhang J, Liu M, Iwahata H, Rogers HB, Woodruff TK. 2017. Doxorubicin has dose-dependent toxicity on mouse ovarian follicle development, hormone secretion, and oocyte maturation. Toxicol Sci 157(2):320–329, PMID: 28329872, https://doi.org/10.1093/toxsci/kfx047.

100. Wang Y, Liu M, Johnson SB, Yuan G, Arriba AK, Zubizarreta ME, et al. 2019. Doxorubicin obliterates mouse ovarian reserve through both primordial follicle atresia and overactivation. Toxicol Appl Pharmacol 381:114714, PMID: 31437492, https://doi.org/10.1016/j.taap.2019.114714.

101. Shi M, Sekulovski N, MacLean JA, Whorton A, Hayashi K. 2019. Prenatal exposure to bisphenol A analogues on female reproductive functions in mice. Toxicol Sci 168(2):561–571, PMID: 30629253, https://doi.org/10.1093/toxsci/kfz014.

102. Sen N, Liu X, Craig ZR. 2015. Short term exposure to di-n-butyl phthalate (DBP) disrupts ovarian function in young CD-1 mice. Reprod Toxicol 53:15–22, PMID: 25765776, https://doi.org/10.1016/j.reprotox.2015.02.012.

103. Liu X, Craig ZR. 2019. Environmentally relevant exposure to dibutyl phthalate disrupts DNA damage repair gene expression in the mouse ovary. Biol Reprod 101(4):854–867, PMID: 31318015, https://doi.org/10.1093/biolre/ioz122.

104. Gupta RK, Miller KP, Babus JK, Flaws JA. 2006. Methoxychlor inhibits growth and induces atresia of antral follicles through an oxidative stress pathway. Toxicol Sci 93(2):382–389, PMID: 16807286, https://doi.org/10.1093/toxsci/kfl052.

105. Craig ZR, Leslie TC, Hatfield KP, Gupta RK, Flaws JA. 2010. Mono-hydroxy methoxychlor alters levels of key sex steroids and steroidogenic enzymes in cultured mouse antral follicles. Toxicol Appl Pharmacol 249(2):107–113, PMID: 20840852, https://doi.org/10.1016/j.taap.2010.09.001.

106. Basavarajappa MS, Craig ZR, Hernandez-Ochoa I, Paulose T, Leslie TC, Flaws JA. 2011. Methoxychlor reduces estradiol levels by altering steroidogenesis and metabolism in mouse antral follicles in vitro. Toxicol Appl Pharmacol 253(3):161–169, PMID: 21514315, https://doi.org/10.1016/j.taap.2011.04.007.

107. Basavarajappa MS, Hernandez-Ochoa I, Wang W, Flaws JA. 2012. Methoxychlor inhibits growth and induces atresia through the aryl hydrocarbon receptor pathway in mouse ovarian antral follicles. Reprod Toxicol 34(1):16–21, PMID: 22484361, https://doi.org/10.1016/j.reprotox.2012.03.007.

108. Patel S, Peretz J, Pan YX, Helferich WG, Flaws JA. 2016. Genistein exposure inhibits growth and alters steroidogenesis in adult mouse antral follicles. Toxicol Appl Pharmacol 293:53–62, PMID: 26792615, https://doi.org/10.1016/j.taap.2015.12.026.

109. Kundu P, Patel S, Meling DD, Deal K, Gao L, Helferich WG, et al. 2018. The effects of dietary levels of genistein on ovarian follicle number and gene expression. Reprod Toxicol 81:132–139, PMID: 30056207, https://doi.org/10.1016/j.reprotox.2018.07.085.

110. Karman BN, Basavarajappa MS, Hannon P, Flaws JA. 2012. Dioxin exposure reduces the steroidogenic capacity of mouse antral follicles mainly at the level of HSD17B1 without altering atresia. Toxicol Appl Pharmacol 264(1):1–12, PMID: 22889882, https://doi.org/10.1016/j.taap.2012.07.031.

111. Karman BN, Basavarajappa MS, Craig ZR, Flaws JA. 2012. 2,3,7,8-Tetrachlorodibenzo-p-dioxin activates the aryl hydrocarbon receptor and alters sex steroid hormone secretion without affecting growth of mouse antral follicles in vitro. Toxicol Appl Pharmacol 261(1):88–96, PMID: 22483799, https://doi.org/10.1016/j.taap.2012.03.015.

112. Patel S, Zhou C, Rattan S, Flaws JA. 2015. Effects of endocrine-disrupting chemicals on the ovary. Biol Reprod 93(1):20, PMID: 26063868, https://doi.org/10.1095/biolreprod.115.130336.

113. Mahalingam S, Gao L, Eisner J, Helferich W, Flaws JA. 2016. Effects of isoliquiritigenin on ovarian antral follicle growth and steroidogenesis. Reprod Toxicol 66:107–114, PMID: 27773742, https://doi.org/10.1016/j.reprotox.2016.10.004.

114. Luan Y, Edmonds ME, Woodruff TK, Kim SY. 2019. Inhibitors of apoptosis protect the ovarian reserve from cyclophosphamide. J Endocrinol 240(2):243–256, PMID: 30530902, https://doi.org/10.1530/JOE-18-0370.

115. Hoogenkamp H, Lewing P. 1982. Superovulation in mice in relation to their age. Vet Q 4(1):47–48, 4, PMID: 1861588, https://doi.org/10.1080/01652176.1982.9693838.

116. Lamas S, Carvalheira J, Gartner F, Amorim I. 2021. C57BL/6J mouse superovulation: schedule and age optimization to increase oocyte yield and reduce animal use. Zygote 29(3):199–203, PMID: 33448261, https://doi.org/10.1017/S0967199420000714.

117. Leesnitzer LM, Parks DJ, Bledsoe RK, Cobb JE, Collins JL, Consler TG, et al. 2002. Functional consequences of cysteine modification in the ligand binding sites of peroxisome proliferator activated receptors by GW9662. Biochemistry 41(21):6640–6650, PMID: 12022867, https://doi.org/10.1021/bi0159581.

118. Seargent JM, Yates EA, Gill JH. 2004. GW9662, a potent antagonist of PPARgamma, inhibits growth of breast tumour cells and promotes the anticancer effects of the PPARgamma agonist rosiglitazone, independently of PPARgamma activation. Br J Pharmacol 143(8):933–937, PMID: 15533890, https://doi.org/10.1038/sj.bjp.0705973.

119. Yoon SY, Kim R, Jang H, Shin DH, Lee JI, Seol D, et al. 2020. Peroxisome proliferator-activated receptor gamma modulator promotes neonatal mouse primordial follicle activation in vitro. Int J Mol Sci 21(9):3120, PMID: 32354153, https://doi.org/10.3390/ijms21093120.

120. Fan H-Y, Liu Z, Shimada M, Sterneck E, Johnson PF, Hedrick SM, et al. 2009. MAPK3/1 (ERK1/2) in ovarian granulosa cells are essential for female fertility. Science 324(5929):938–941, PMID: 19443782, https://doi.org/10.1126/science.1171396.

121. Tatum-Gibbs K, Wambaugh JF, Das KP, Zehr RD, Strynar MJ, Lindstrom AB, et al. 2011. Comparative pharmacokinetics of perfluorononanoic acid in rat and mouse. Toxicology 281(1–3):48–55, PMID: 21237237, https://doi.org/10.1016/j.tox.2011.01.003.

122. US EPA (US Environmental Protection Agency). Benchmark Dose Tools (BMDS) Online. https://bmdsonline.epa.gov/ [accessed 14 April 2023].

123. US EPA. 2012. Benchmark Dose Technical Guidance. https://www.epa.gov/sites/default/files/2015-01/documents/benchmark_dose_guidance.pdf [accessed 14 April 2023].

124. Dourson M, Ewart L, Fitzpatrick SC, Barros SBM, Mahadevan B, Hayes AW. 2022. The future of uncertainty factors with in vitro studies using human cells. Toxicol Sci 186(1):12–17, PMID: 34755872, https://doi.org/10.1093/toxsci/kfab134.

125. Walton K, Dorne JL, Renwick AG. 2001. Uncertainty factors for chemical risk assessment: interspecies differences in glucuronidation. Food Chem Toxicol 39(12):1175–1190, PMID: 11696391, https://doi.org/10.1016/s0278-6915(01)00088-6.

126. Committee on Gynecologic Practice, American Society for Reproductive Medicine. 2019. Infertility workup for the women's health specialist: ACOG Committee opinion, number 781. Obstet Gynecol 133(6):e377–e384, PMID: 31135764, https://doi.org/10.1097/AOG.0000000000003271.

127. World Health Organization. 2022. WHO Fact Sheets of Infertility. https://www.who.int/news-room/fact-sheets/detail/infertility [accessed 9 January 2023].

128. US Centers for Disease Control and Prevention. Infertility. https://www.cdc.gov/nchs/fastats/infertility.html [accessed 9 January 2023].

129. Bala R, Singh V, Rajender S, Singh K. 2021. Environment, lifestyle, and female infertility. Reprod Sci 28(3):617–638, PMID: 32748224, https://doi.org/10.1007/s43032-020-00279-3.

130. Ding N, Harlow SD, Randolph JF Jr., Loch-Caruso R, Park SK. 2020. Perfluoroalkyl and polyfluoroalkyl substances (PFAS) and their effects on the ovary. Hum Reprod Update 26(5):724–752, PMID: 32476019, https://doi.org/10.1093/humupd/dmaa018.

131. Post GB, Louis JB, Lippincott RL, Procopio NA. 2013. Occurrence of perfluorinated compounds in raw water from New Jersey public drinking water systems. Environ Sci Technol 47(23):13266–13275, PMID: 24187954, https://doi.org/10.1021/es402884x.

132. Cai M, Yang H, Xie Z, Zhao Z, Wang F, Lu Z, et al. 2012. Per- and polyfluoroalkyl substances in snow, lake, surface runoff water and coastal seawater in Fildes Peninsula, King George Island, Antarctica. J Hazard Mater 209-210:335–342, PMID: 22305203, https://doi.org/10.1016/j.jhazmat.2012.01.030.

133. Wignall JA, Shapiro AJ, Wright FA, Woodruff TJ, Chiu WA, Guyton KZ, et al. 2014. Standardizing benchmark dose calculations to improve science-based decisions in human health assessments. Environ Health Perspect 122(5):499–505, PMID: 24569956, https://doi.org/10.1289/ehp.1307539.

134. Brescia S, Alexander-White C, Li H, Cayley A. 2023. Risk assessment in the 21st century: where are we heading? Toxicol Res (Camb) 12(1):1–11, PMID: 36866215, https://doi.org/10.1093/toxres/tfac087.

135. Health Canada. 2021. Science Approach Document: Bioactivity Exposure Ratio: Application in Priority Setting and Risk Assessment, Part I No. 10. https://www.canada.ca/en/environment-climate-change/services/evaluating-existing-substances/science-approach-document-bioactivity-exposure-ratio-application-priority-setting-risk-assessment.html [accessed 15 July 2024].

136. Baltazar MT, Cable S, Carmichael PL, Cubberley R, Cull T, Delagrange M, et al. 2020. A next-generation risk assessment case study for coumarin in cosmetic products. Toxicol Sci 176(1):236–252, PMID: 32275751, https://doi.org/10.1093/toxsci/kfaa048.

137. Niu S, Cao Y, Chen R, Bedi M, Sanders AP, Ducatman A, et al. 2023. A state-of-the-science review of interactions of per- and polyfluoroalkyl substances (PFAS) with renal transporters in health and disease: implications for population variability in PFAS toxicokinetics. Environ Health Perspect 131(7):076002, PMID: 37418334, https://doi.org/10.1289/EHP11885.

138. Nakagawa H, Terada T, Harada KH, Hitomi T, Inoue K, Inui K-I, et al. 2009. Human organic anion transporter hOAT4 is a transporter of perfluorooctanoic acid. Basic Clin Pharmacol Toxicol 105(2):136–138, PMID: 19371258, https://doi.org/10.1111/j.1742-7843.2009.00409.x.

139. Bardot O, Aldridge TC, Latruffe N, Green S. 1993. PPAR-RXR heterodimer activates a peroxisome proliferator response element upstream of the bifunctional enzyme gene. Biochem Biophys Res Commun 192(1):37–45, PMID: 8386511, https://doi.org/10.1006/bbrc.1993.1378.

140. Ferre P. 2004. The biology of peroxisome proliferator-activated receptors: relationship with lipid metabolism and insulin sensitivity. Diabetes 53(suppl 1):S43–S50, PMID: 14749265, https://doi.org/10.2337/diabetes.53.2007.s43.

141. Desvergne B, Wahli W. 1999. Peroxisome proliferator-activated receptors: nuclear control of metabolism. Endocr Rev 20(5):649–688, PMID: 10529898, https://doi.org/10.1210/edrv.20.5.0380.

142. Komar CM. 2005. Peroxisome proliferator-activated receptors (PPARs) and ovarian function–implications for regulating steroidogenesis, differentiation, and tissue remodeling. Reprod Biol Endocrinol 3:41, PMID: 16131403, https://doi.org/10.1186/1477-7827-3-41.

143. Mu YM, Yanase T, Nishi Y, Waseda N, Oda T, Tanaka A, et al. 2000. Insulin sensitizer, troglitazone, directly inhibits aromatase activity in human ovarian granulosa cells. Biochem Biophys Res Commun 271(3):710–713, PMID: 10814527, https://doi.org/10.1006/bbrc.2000.2701.

144. Fan W, Yanase T, Morinaga H, Mu Y-M, Nomura M, Okabe T, et al. 2005. Activation of peroxisome proliferator-activated receptor-gamma and retinoid X receptor inhibits aromatase transcription via nuclear factor-kappaB. Endocrinology 146(1):85–92, PMID: 15459115, https://doi.org/10.1210/en.2004-1046.

145. Mu YM, Yanase T, Nishi Y, Takayanagi R, Goto K, Nawata H. 2001. Combined treatment with specific ligands for PPARgamma: RXR nuclear receptor system markedly inhibits the expression of cytochrome P450arom in human granulosa cancer cells. Mol Cell Endocrinol 181(1–2):239–248, PMID: 11476957, https://doi.org/10.1016/s0303-7207(00)00457-3.

146. Lovekamp-Swan T, Jetten AM, Davis BJ. 2003. Dual activation of PPARalpha and PPARgamma by mono-(2-ethylhexyl) phthalate in rat ovarian granulosa cells. Mol Cell Endocrinol 201(1–2):133–141, PMID: 12706301, https://doi.org/10.1016/s0303-7207(02)00423-9.

147. Toda K, Okada T, Miyaura C, Saibara T. 2003. Fenofibrate, a ligand for PPARalpha, inhibits aromatase cytochrome P450 expression in the ovary of mouse. J Lipid Res 44(2):265–270, PMID: 12576508, https://doi.org/10.1194/jlr.M200327-JLR200.

148. Espey LL. 1980. Ovulation as an inflammatory reaction–a hypothesis. Biol Reprod 22(1):73–106, PMID: 6991013, https://doi.org/10.1095/biolreprod22.1.73.

149. Duffy DM, Ko C, Jo M, Brannstrom M, Curry TE. 2019. Ovulation: parallels with inflammatory processes. Endocr Rev 40(2):369–416, PMID: 30496379, https://doi.org/10.1210/er.2018-00075.

150. Richards JS, Ascoli M. 2018. Endocrine, paracrine, and autocrine signaling pathways that regulate ovulation. Trends Endocrinol Metab 29(5):313–325, PMID: 29602523, https://doi.org/10.1016/j.tem.2018.02.012.

151. Liu Z, de Matos DG, Fan HY, Shimada M, Palmer S, Richards JS. 2009. Interleukin-6: an autocrine regulator of the mouse cumulus cell-oocyte complex expansion process. Endocrinology 150(7):3360–3368, PMID: 19299453, https://doi.org/10.1210/en.2008-1532.

152. Wang S, Yang H, Fu Y, Teng X, Wang C, Xu W. 2022. The key role of peroxisomes in follicular growth, oocyte maturation, ovulation, and steroid biosynthesis. Oxid Med Cell Longev 2022:7982344, PMID: 35154572, https://doi.org/10.1155/2022/7982344.

153. Marei WF, Wathes DC, Fouladi-Nashta AA. 2010. Impact of linoleic acid on bovine oocyte maturation and embryo development. Reproduction 139(6):979–988, PMID: 20215338, https://doi.org/10.1530/REP-09-0503.

154. Paczkowski M, Silva E, Schoolcraft WB, Krisher RL. 2013. Comparative importance of fatty acid beta-oxidation to nuclear maturation, gene expression, and glucose metabolism in mouse, bovine, and porcine cumulus oocyte complexes. Biol Reprod 88(5):111, PMID: 23536372, https://doi.org/10.1095/biolreprod.113.108548.

155. Wu LL-Y, Dunning KR, Yang X, Russell DL, Lane M, Norman RJ, et al. 2010. High-fat diet causes lipotoxicity responses in cumulus-oocyte complexes and decreased fertilization rates. Endocrinology 151(11):5438–5445, PMID: 20861227, https://doi.org/10.1210/en.2010-0551.

156. National Toxicology Program. 2019. Toxicity studies of perfluoroalkyl sulfonates administered by gavage to Sprague Dawley (Hsd: Sprague Dawley SD) rats (revised). Toxic Rep Ser (96):NTP-TOX-96, PMID: 33533754, https://doi.org/10.22427/NTP-TOX-96.

157. Vierke L, Moller A, Klitzke S. 2014. Transport of perfluoroalkyl acids in a water-saturated sediment column investigated under near-natural conditions. Environ Pollut 186:7–13, PMID: 24333660, https://doi.org/10.1016/j.envpol.2013.11.011.

158. Lam JC, Lyu J, Kwok KY, Lam PK. 2016. Perfluoroalkyl substances (PFASs) in marine mammals from the South China Sea and their temporal changes 2002–2014: concern for alternatives of PFOS? Environ Sci Technol 50(13):6728–6736, PMID: 26889942, https://doi.org/10.1021/acs.est.5b06076.

159. Boiteux V, Dauchy X, Bach C, Colin A, Hemard J, Sagres V, et al. 2017. Concentrations and patterns of perfluoroalkyl and polyfluoroalkyl substances in a river and three drinking water treatment plants near and far from a major production source. Sci Total Environ 583:393–400, PMID: 28117151, https://doi.org/10.1016/j.scitotenv.2017.01.079.

160. Zhao P, Xia X, Dong J, Xia N, Jiang X, Li Y, et al. 2016. Short- and long-chain perfluoroalkyl substances in the water, suspended particulate matter, and surface sediment of a turbid river. Sci Total Environ 568:57–65, PMID: 27285797, https://doi.org/10.1016/j.scitotenv.2016.05.221.

161. Gagliano E, Sgroi M, Falciglia PP, Vagliasindi FGA, Roccaro P. 2020. Removal of poly- and perfluoroalkyl substances (PFAS) from water by adsorption: role of PFAS chain length, effect of organic matter and challenges in adsorbent regeneration. Water Res 171:115381, PMID: 31923761, https://doi.org/10.1016/j.watres.2019.115381.

162. D'Agostino LA, Mabury SA. 2017. Aerobic biodegradation of 2 fluorotelomer sulfonamide-based aqueous film-forming foam components produces perfluoroalkyl carboxylates. Environ Toxicol Chem 36(8):2012–2021, PMID: 28145584, https://doi.org/10.1002/etc.3750.

163. Nicole W. 2020. Breaking it down: estimating short-chain PFAS half-lives in a human population. Environ Health Perspect 128(11):114002, PMID: 33174763, https://doi.org/10.1289/EHP7853.

164. Zheng G, Eick SM, Salamova A. 2023. Elevated levels of ultrashort- and short-chain perfluoroalkyl acids in US homes and people. Environ Sci Technol 57(42):15782–15793, PMID: 37818968, https://doi.org/10.1021/acs.est.2c06715.

165. Brendel S, Fetter É, Staude C, Vierke L, Biegel-Engler A. 2018. Short-chain perfluoroalkyl acids: environmental concerns and a regulatory strategy under REACH. Environ Sci Eur 30(1):9, PMID: 29527446, https://doi.org/10.1186/s12302-018-0134-4.

166. Bischel HN, Macmanus-Spencer LA, Zhang C, Luthy RG. 2011. Strong associations of short-chain perfluoroalkyl acids with serum albumin and investigation of binding mechanisms. Environ Toxicol Chem 30(11):2423–2430, PMID: 21842491, https://doi.org/10.1002/etc.647.

167. Chen YM, Guo LH. 2009. Fluorescence study on site-specific binding of perfluoroalkyl acids to human serum albumin. Arch Toxicol 83(3):255–261, PMID: 18854981, https://doi.org/10.1007/s00204-008-0359-x.

168. Solan ME, Senthilkumar S, Aquino GV, Bruce ED, Lavado R. 2022. Comparative cytotoxicity of seven per- and polyfluoroalkyl substances (PFAS) in six human cell lines. Toxicology 477:153281, PMID: 35933025, https://doi.org/10.1016/j.tox.2022.153281.

169. Palazzolo S, Caligiuri I, Sfriso AA, Mauceri M, Rotondo R, Campagnol D, et al. 2022. Early warnings by liver organoids on short- and long-chain PFAS toxicity. Toxics 10(2):91, PMID: 35202277, https://doi.org/10.3390/toxics10020091.

170. Houck KA, Patlewicz G, Richard AM, Williams AJ, Shobair MA, Smeltz M, et al. 2021. Bioactivity profiling of per- and polyfluoroalkyl substances (PFAS) identifies potential toxicity pathways related to molecular structure. Toxicology 457:152789, PMID: 33887376, https://doi.org/10.1016/j.tox.2021.152789.

171. Corton JC, Peters JM, Klaunig JE. 2018. The PPARalpha-dependent rodent liver tumor response is not relevant to humans: addressing misconceptions. Arch Toxicol 92(1):83–119, PMID: 29197930, https://doi.org/10.1007/s00204-017-2094-7.

172. Pap A, Cuaranta-Monroy I, Peloquin M, Nagy L. 2016. Is the mouse a good model of human PPARgamma-related metabolic diseases? Int J Mol Sci 17(8):1236, PMID: 27483259, https://doi.org/10.3390/ijms17081236.

173. Palmer CN, Hsu MH, Griffin KJ, Raucy JL, Johnson EF. 1998. Peroxisome proliferator activated receptor-alpha expression in human liver. Mol Pharmacol 53(1):14–22, PMID: 9443928.

174. Lin P-ID, Cardenas A, Hauser R, Gold DR, Kleinman KP, Hivert M-F, et al. 2020. Dietary characteristics associated with plasma concentrations of per- and polyfluoroalkyl substances among adults with pre-diabetes: cross-sectional results from the Diabetes Prevention Program Trial. Environ Int 137:105217, PMID: 32086073, https://doi.org/10.1016/j.envint.2019.105217.

175. Li R, Guo C, Lin X, Chan TF, Su M, Zhang Z, et al. 2022. Integrative omics analysis reveals the protective role of vitamin C on perfluorooctanoic acid-induced hepatotoxicity. J Adv Res 35:279–294, PMID: 35024202, https://doi.org/10.1016/j.jare.2021.04.003.

176. Orisaka M, Tajima K, Tsang BK, Kotsuji F. 2009. Oocyte-granulosa-theca cell interactions during preantral follicular development. J Ovarian Res 2(1):9, PMID: 19589134, https://doi.org/10.1186/1757-2215-2-9.

177. Eppig JJ, Pendola FL, Wigglesworth K, Pendola JK. 2005. Mouse oocytes regulate metabolic cooperativity between granulosa cells and oocytes: amino acid transport. Biol Reprod 73(2):351–357, PMID: 15843493, https://doi.org/10.1095/biolreprod.105.041798.

178. Su Y-Q, Sugiura K, Wigglesworth K, O'Brien MJ, Affourtit JP, Pangas SA, et al. 2008. Oocyte regulation of metabolic cooperativity between mouse cumulus cells and oocytes: BMP15 and GDF9 control cholesterol biosynthesis in cumulus cells. Development 135(1):111–121, PMID: 18045843, https://doi.org/10.1242/dev.009068.

179. Mohan M, Malayer JR, Geisert RD, Morgan GL. 2002. Expression patterns of retinoid X receptors, retinaldehyde dehydrogenase, and peroxisome proliferator activated receptor gamma in bovine preattachment embryos. Biol Reprod 66(3):692–700, PMID: 11870076, https://doi.org/10.1095/biolreprod66.3.692.

180. Xiao S, Zhang J, Romero MM, Smith KN, Shea LD, Woodruff TK. 2015. In vitro follicle growth supports human oocyte meiotic maturation. Sci Rep 5:17323, PMID: 26612176, https://doi.org/10.1038/srep17323.